JOURNAL OF COLLOID AND INTERFACE SCIENCE **187,** 62–82 (1997)
ARTICLE NO. CS964539

Surface Precipitation of Co(II)(aq) on Al_2O_3

STEVEN N. TOWLE,*,†,[1] JOHN R. BARGAR,* GORDON E. BROWN, JR.,*,‡ AND GEORGE A. PARKS*

*Department of Geological and Environmental Sciences, †Department of Materials Science and Engineering, and ‡Stanford Synchrotron Radiation Laboratory, Stanford University, Stanford, California 94305-2115

Received May 20, 1996; accepted July 30, 1996

Surface precipitation is an important process in many areas of science and technology, including modeling contaminant segregation from groundwater to solid phases and dispersion of active phases on catalyst supports. XAFS, TEM, and XPS measurements of Co(II) sorbed on Al_2O_3 demonstrate that surface precipitates have formed from solutions that are undersaturated with respect to any known bulk solid phase. The precipitates have a structure similar to that of $Co(OH)_2(s)$, but are disordered and have a high concentration of Co vacancies. The data plus thermodynamic reasoning have been used to analyze the plausibility of various models for surface precipitation and to show that for Co(II)/Al_2O_3 it occurs by forming a double-hydroxide phase containing substrate-derived Al(III) ions. This idea was corroborated by mixing aqueous solutions of Al(III) and Co(II) at the pH and concentration of the sorption samples, forming a stable colloidal precipitate that is less soluble than either $Al(OH)_3$ or $Co(OH)_2$. The Co XAFS of this material was similar to that of the sorption samples. Successful quantitative models of metal ion transport in groundwater need to include the possibility of forming ternary and higher order precipitates that include ions derived from sparingly soluble solids. For catalyst impregnation, surface coprecipitation can prevent production of a well-dispersed precursor material. © 1997 Academic Press

Key Words: **surface precipitation; coprecipitation; double hydroxide; cobalt(II); alumina; sorption; polynuclear complex; XAFS; TEM.**

INTRODUCTION

When cations are sorbed on oxide surfaces at high surface concentration, it has been proposed that a transition takes place from mononuclear adsorption, to multinuclear adsorption, and finally to surface precipitation (1–3). Such a transition can account for the fact that, in oxide systems, the sorption capacity of the substrate rarely saturates; i.e., it is not limited by occupation of all available surface sites, as is predicted by standard surface complexation models (4). Also, a transition of this type can account for existing spectroscopic data which suggest that sorbing metal ions form hydroxo-bridged clusters at high surface coverages (1). In the present study, the details of this transition are investigated for the Co(II)/Al_2O_3 system using several probes of molecular structural and composition, and a review is made of the various processes that may cause surface precipitation.

In past work, the term ''surface precipitation'' has been used to describe various precipitation phenomena that take place at a solid–water interface, such as heterocoagulation and heterogeneous nucleation of a precipitate phase. In this paper, however, we use it in a strict sense of ''surface-induced precipitation,'' i.e., the formation of a precipitate under solution conditions that would, in the absence of the substrate solid, be undersaturated with respect to any known solid phase. The term ''adsorption'' is used to refer to the formation of metal ion surface complexes, while ''uptake'' refers to the partitioning of a dissolved species to a solid phase, irrespective of the sorption mechanism.

An understanding of when and how precipitates form at surfaces is important in a number of areas that are of scientific and technological importance. For example, an understanding of the process of surface precipitation is required for accurate quantitative modeling of metal ion uptake, especially at the highest concentrations (5, 6). Unless the numbers of surface sites, metal ions, protons, and so forth participating in the reaction are known, extrapolation of a model to conditions where it has not been calibrated can give results that are off by orders of magnitude (7). In the modeling of contaminant transport in groundwater, for instance, the widely varying conditions that exist in the field cannot generally be reproduced in the lab. In another example, such knowledge would aid in the prediction of contamination tolerances for cations in aqueous solutions used in integrated circuit processing. In addition, there is evidence that the process by which cations are sorbed, be it surface precipitation or adsorption, affects the subsequent sorption of anions (8).

The morphology and distribution of surface precipitates are critical factors in certain technological applications, such as the preparation of heterogeneous catalysts and

[1] To whom correspondence should be addressed.

0021-9797/97 $25.00

the formation of coatings. In the preparation of oxide-supported transition metal catalysts, such as Co/Mo/Al_2O_3 used for hydrodesulfurization and Co/Al_2O_3 for Fischer-Tropsch synthesis, the dispersion of the catalytic phase over the oxide surface is one of the main factors controlling the activity of the catalyst. For smaller particles on the surface, a larger proportion of metal atoms can act as active sites. A number of techniques are used in catalyst preparation to control the dispersion, but one influence is the size of the precursor clusters (9), which are often formed in an aqueous sorption step. However, little work has been done in this area (10), in part because it is rather difficult to characterize the distribution of the adsorbed species. These issues are also important for other supported heterogeneous catalysis systems (11), such as supported oxide catalysts. An aqueous sorption step is also the usual method used for producing coatings on titanium dioxide pigment particles in paints. In this case, the critical issues are the physical completeness and integrity of the coating and its effectiveness as a chemical barrier (12).

In this study, we have prepared samples in which Al_2O_3 powder has been equilibrated with Co(II) aqueous solutions of concentrations ranging from well undersaturated to oversaturated with respect to bulk phase precipitation in the absence of a solid sorbent. These samples have been analyzed with X-ray absorption fine structure (XAFS), X-ray photoelectron spectroscopy (XPS), and transmission electron microscopy (TEM). This combination of techniques can reveal the presence of surface precipitates and also yield information about their morphology and structure. The characterization is comprehensive enough to justify a reexamination of some of the hypotheses that have been offered for surface precipitation.

XAFS spectroscopy, in particular, is well suited to addressing the structure, composition, and distribution of the sorbate because it is element specific; thus it is quite sensitive to surface species if a given element occurs only at a surface. In addition, XAFS is sensitive to both the chemical state and the local atomic structure and can be performed on sorption samples *in situ*, that is, with bulk water present, providing unique information about chemical species at solid–water interfaces. Both the extended XAFS (EXAFS) and near-edge region (XANES, or X-ray absorption near-edge structure) are analyzed, as they provide complementary information about different aspects of the local structure around sorbed Co. TEM is able to provide real-space structural and morphological information about the substrate (sorbent) and the sorbate and, in combination with XAFS, may be used to distinguish between polynuclear surface complexes and surface precipitates (13), which is difficult with XAFS alone. XPS provides additional information about the composition, oxidation state, and bonding of the sorption complex, as well as quantitative information about surface sorption density.

Cobalt(II) and Al_2O_3 form an advantageous system for study for several reasons. Cobalt hydrolysis and $Co(OH)_2$ precipitation have been extensively studied in the past, so reliable thermodynamic data are available (14, 15). In addition, the Co*K* edge is at a convenient energy for XAFS data collection because at the Co*K* edge (7700 eV) the X-rays are sufficiently penetrating to perform *in situ* experiments and because this energy is near the maximum in the spectral brilliance of the synchrotron. The alumina powder we used (Linde-A) has the advantage that its surface and acid/base properties have already been thoroughly characterized (2). Furthermore, the Co(II)/Al_2O_3 system has been the subject of considerable previous study, including XAFS characterization (16–18), due to its importance as a catalyst and its relevance to natural systems. Al_2O_3 can serve as an analog for hydrous alumina gel, crystalline aluminum oxyhydroxides, and aluminol layers in clays, some of the more common surfaces found in natural environments.

BACKGROUND

A great deal of previous research has examined the manner in which aqueous metal ions sorb on solid oxide surfaces, and a number of thermodynamic models of sorption have been proposed. Successful models need to account for the observed dependence of sorbate uptake on the activity of each of the reacting species, which for the simplest systems at low surface concentrations consist of dissolved metal ions, surface functional groups, and hydrogen or hydroxyl ions. Such models are expressed as one or more reactions of the general type

$$x\underline{\mathrm{AlOH}} + y\mathrm{Co}^{2+}(\mathrm{aq}) + z\mathrm{H_2O} = \underline{\mathrm{AlO}_x\mathrm{Co}_y(\mathrm{OH})_z}^{(2y-x-z)+} + (x+z)\mathrm{H}^+(\mathrm{aq}) \quad [1]$$

where $\underline{\mathrm{AlO}}$ represents a surface functional group. By altering the stoichiometric coefficients of the various species, multidentate complexes, surface hydroxylation, or surface polymer formation may be described, with each proposed reaction having its own equilibrium constant. Typically, two or more such reactions are used to reproduce the observed overall proton stoichiometry associated with metal ion sorption, which is usually noninteger. However, macroscopic uptake data alone cannot distinguish among models that propose different sets of reactions (19).

These models are basically Langmuirian in that they assume a constant number of identical surface sites of a particular type and that no interactions occur among neighboring adsorbed metal ion complexes. While these assumptions may hold at low surface concentration ($\ll$1 monolayer), at higher

surface concentrations it has been observed that ''Langmuirian'' behavior cannot account for the measured extent of uptake (4).

The conceptually simplest approach to improving this model is to use the mathematical framework of a Langmuirian-type model, but to suppose that as the sorption density increases the surface complexes become ever larger. Co(II) multinuclear complexes are justifiable because they are known to exist in solution, though their concentrations are significant only in solutions that are oversaturated with respect to $Co(OH)_2(s)$ (20). In this work, Co(II) multinuclear complexes constituted less than 0.001% of the Co in solution, even at the highest pH and concentration.

One problem with using this approach to model sorption at high surface densities (i.e., where the sorbate surface concentration is higher than the concentration of surface sites) is that each reaction that forms a successively larger complex requires its own equilibrium constant, leading to a large number of fitted parameters. Also, this type of model does not account for data which suggest that precipitates can form on the surface under conditions where the bulk solution remains undersaturated.

Studies using spectroscopic, electrophoretic mobility, and uptake techniques have all provided evidence that the presence of a sorbent solid can induce precipitation from bulk solutions that are undersaturated with respect to any known phase. Benjamin (8) showed that when the ratio of solid sorbent (hydrous ferric oxide, or HFO) to sorbing metal ion (Co(II), Cd(II), Cu(II), or Zn(II)) was held constant, the fractional uptake changed when the total concentrations of sorbents and sorbates were varied, an effect that would not be expected for a mononuclear sorption process. Furthermore, the pH dependency of anion (SeO_4^- and CrO_4^-) adsorption on sorbents that had already been reacted with metal ions was found to be consistent with surface precipitation of metal hydroxides at the higher metal ion and solid concentrations studied but with true adsorption at lower concentrations. In an XAFS study, Charlet and Manceau (21) concluded that Cr(III) sorbed on HFO had a local structure very similar to that of hydrous chromium oxide, though the solution was undersaturated with respect to $Cr(OH)_3$. This local structure was different from that seen when Cr and Fe were coprecipitated at the same overall Cr/Fe concentration ratio, in which case the structure was nearly identical to that of HFO. Bleam and McBride (22) studied the sorption of Mn(II) and Mg(II) on goethite (FeOOH) and boehmite (AlOOH), and concluded that a ''clustering'' mechanism was responsible for sorption in all cases except for Mg(II)/goethite. These conclusions were based on EPR data in the case of Mn(II), but only on electrophoretic mobility data for Mg(II).

Several other studies of metal ion/oxide sorption systems have suggested that surface precipitates may be present, but they have not been as definitive as the studies cited above. Much of the original thinking about precipitation below saturation came from James and Healy (23), who suggested that a surface precipitation mechanism could explain the variations in surface charge with increasing pH in the $Co(II)/SiO_2$ and $Co(II)/TiO_2$ systems. Tewari and Lee (24) concluded based on XPS data that a surface precipitate of $Co(OH)_2$ had formed on Al_2O_3. An XAFS study by Scheidegger *et al.* (25) suggested the formation of a $Ni(OH)_2$-like phase when Ni(II) sorbs on pyrophyllite (a layered alumino-silicate). This group later confirmed the result using TEM. Dzombak and Morel (26), in a reanalysis of the work of Kinniburgh and Jackson (27) on the Zn(II)/HFO system, concluded that the uptake data could be best explained by a surface precipitation model. Another reanalysis of previous data was conducted by Charlet and Manceau (28), who suggested that in a number of past studies of Co(II) and Ni(II) adsorption on silicates, XAFS data could be best explained by a mechanism of neoformation, or reprecipitation, of clay-like structures involving both the transition metal cation and Si derived from the different sorbents. This idea, however, is disputed by O'Day *et al.* (29, 30), who concluded that at high sorption densities Co(II) sorbs on kaolinite and quartz as a hydroxide precipitate whose structure is not consistent with the neoformation mechanism proposed by Charlet and Manceau.

In order to adequately explain evidence that surface precipitation (i.e., precipitation from undersaturated solutions, as defined previously) can occur, several models have been proposed. James and Healy (23), in the same study in which they presented their electrokinetic data, proposed a thermodynamic model in which surface potential gradients affect the permittivity of the aqueous medium and hence the solvation energy of the ions, but not the properties of the solids likely to precipitate, with the net effect of allowing precipitation at the interface while the bulk solution remains undersaturated. Ananthapadmanabhan and Somasundaran (31) suggested that as the pH increases, the charging behavior of the solid induces a disproportionate increase in the hydroxyl ion concentration in the vicinity of the interface, thus causing precipitation of hydroxide. These authors did not, however, propose a quantitative model, nor did they explain why the metal ion concentration in the interface region would be unaffected by the surface charging. Farley *et al.* (4) proposed a model which is entirely different in concept, with the objective of showing why surface coverage typically does not reach a maximum at high concentration. In this model, the activity of the sorbing metal cation component of the precipitate phase is made lower by formation of a solid solution with the sorbent material. Katz and Hayes (3) proposed a modification of this model that allows multinuclear complexation as well as surface precipitation.

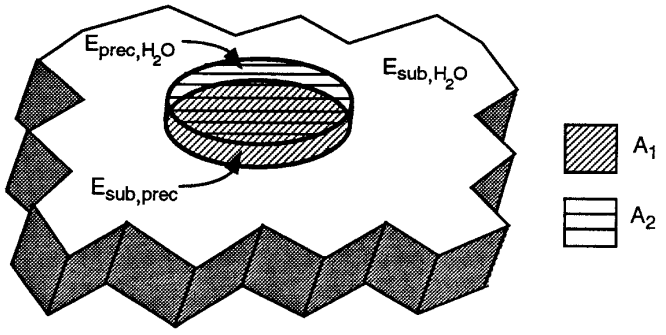

FIG. 1. Schematic illustrating the contributions of surface energies to a precipitate particle forming on the substrate. See text for definition of variables.

In principle, precipitation could also be induced by a net decrease in surface energy, if the following inequality holds:

$$A_1 E_{\text{sub,prec}} + A_2 E_{\text{prec,H}_2\text{O}} \leq A_1 E_{\text{sub,H}_2\text{O}}. \qquad [2]$$

$E_{\text{sub,prec}}$ is the interfacial energy between the substrate and the precipitate, $E_{\text{prec,H}_2\text{O}}$ is the interfacial energy between the precipitate and water, and $E_{\text{sub,H}_2\text{O}}$ is the interfacial energy between the substrate and water. A_1 and A_2 are the relative areas of the interfaces and would be equal in the planar geometry illustrated in Fig. 1. In a crack or micropore, however, A_1 might be much greater than A_2. For surface energy to induce precipitation, the net decrease in free energy contributed by the surface energies must counterbalance the net increase in free energy contributed by transforming the undersaturated aqueous species to the precipitate phase.

Another possible explanation for surface precipitation in sorption experiments is a kinetic effect associated with dropwise addition of base during titration. According to this idea, the addition of a droplet of base, even in a strongly stirred suspension, may cause a momentary oversaturation of the hydroxide phase at the boundary between the dissipating droplet and the rest of the suspension. Such oversaturation would allow precipitates to be formed by heterogeneous nucleation at the sorbent surface. The sorbent surface may also kinetically inhibit the precipitate from dissolving, perhaps because of inadequate mixing in the pore spaces of the material, so a thermodynamically unstable precipitate might persist through the duration of the adsorption experiment. One way of avoiding this problem is to add the base coulommetrically via the electrochemical half-reaction:

$$2H_2O(l) + 2e^- = H_2(g) + 2OH^-(aq). \qquad [3]$$

The cell is completed by the electrochemical dissolution of a metal, such as silver. Because the hydroxyl ions are produced over a large area and may be added as slowly as desired (as opposed to the sudden addition of a concentrated quantity of base in a droplet), the oversaturation problem can usually be eliminated. Of the studies discussed above, only the Cr(III)/HFO work of Charlet and Manceau (21) used coulommetric titration, so in principle this kinetic effect could be the cause of surface precipitation in all of the other work.

In summary, the thermodynamic models that have been proposed to explain the phenomenon of surface precipitation fall into two categories: those that explain the change in precipitation behavior by invoking a change in the properties of the solution in the vicinity of the interface, and those that explain precipitation by considering changes in the precipitating solid. The first type includes the model of James and Healy (23) as well as ideas such as those of Ananthapadmanabhan and Somasundaran. The solid solution model of Farley *et al.* (4) and the surface-energy effect are of the latter type. Katz and Hayes's (3) model is in principle analogous to the solid solution model of Farley *et al.*, but instead of proposing that the formation of a solid solution causes the activity of the precipitating component to be less than unity, they simply define the activity to be the mole fraction of all the sorbed metal which is contained in the precipitate. No physical explanation is offered for this definition. As the following argument will show, only variations in the activity of the sorbing ion in the precipitate phase (as opposed to the solution phase) can induce precipitation, so long as the interface remains in thermodynamic equilibrium with the bulk solution.

The simplest conceptual way of showing this is to imagine an isolated thermodynamic system (i.e., no exchange of heat, work or mass) consisting of two regions, as shown in Fig. 2. One region is bulk aqueous solution containing Co^{2+} and OH^- and the other is aqueous solution in the vicinity of the oxide–water interface. We make two assumptions: first, the interface region is in equilibrium with the bulk solution, and

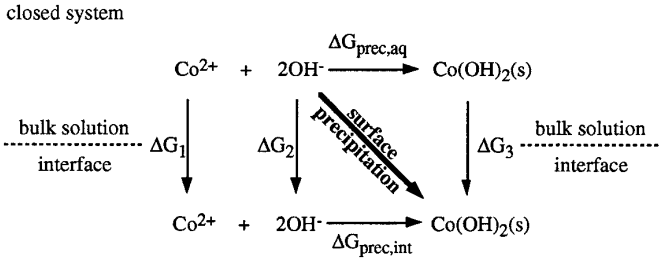

FIG. 2. Illustration of alternative reaction paths for the formation of a surface precipitate. ΔG_1 and ΔG_2 are the free energies associated with transition of an ion from aqueous solution to the interface region; ΔG_3 is the free energy associated with the transition of a solid precipitate from the bulk solution to the interface region and, for macroscopic precipitate particles, should be near zero. ΔG_{prec} is the free energy of the precipitation reaction; the subscripts aq and int indicate its values in the bulk solution and at the interface, respectively.

second, the properties of the solid are not affected by its being in the vicinity of the interface, so long as the solid particles are macroscopic in size (i.e., at least several nanometers). As changes in thermodynamic state variables (in this case, the free energy change associated with surface precipitation) are independent of the chosen reaction path, we can consider the precipitation of a solid in the interface region to be equivalent to formation of the solid elsewhere, and then the transportation of that solid to the interface. Since the properties of the solid are assumed to be unaffected by the interface, the second step involves no change in free energy. As a consequence, if the solution is exactly at equilibrium with a particular solid, it will also be exactly at equilibrium with a surface precipitate composed of that solid. Intermediate states falling on alternate reactions paths, such as ions in the interfacial region, as shown in Fig. 2, have no effect on the free energy of precipitation. A corollary to this argument is that, since there is no net transfer of charge when the solid is moved from one region to the other, the electrification of the interface cannot induce precipitation, so long as the solid formed has no space charge.

This conceptual argument can be couched in formal thermodynamic terms, as follows. Assume, initially, that the interface is uncharged so electrical effects can be neglected. In aqueous solution, the chemical potential μ_{aq} of an ion is defined as

$$\mu_{aq} = \mu^0 + RT \ln a_{aq}, \quad [4]$$

where μ^0 is the standard molar chemical potential of the ion in some reference state, R is the gas constant, T is the absolute temperature, and a_{aq} is the activity of the ion in question. If it is assumed that the interface region is in thermodynamic equilibrium with the bulk solution, the chemical potential at the interface must be the same as in bulk solution, giving

$$a_{aq} = a_{int}. \quad [5]$$

Naturally, the same argument would apply for both cations and anions. Since the activities are the same at the interface and in the bulk, the degree of saturation with respect to a precipitate will be the same.

However, the activity coefficients, γ_i, defined as the activity of a species divided by its mole fraction (concentration), will in general be different in the interface region versus the bulk aqueous solution. This may be most clearly seen by comparing the activity coefficients in the two regions at some particular concentration, X_i. Supposing that, as James and Healy suggest, the permittivity of water is lower in the interface region than in the bulk, the energy of solvation of the ion will also be less, i.e., the partial molar free energy of mixing of the metal ion will be less negative:

$$\Delta\bar{G}^M_{aq} < \Delta\bar{G}^M_{int}. \quad [6]$$

Note that since these free energies of mixing are different, the two regions are not in equilibrium. From the definition of the partial molar free energy of mixing (32),

$$\Delta\bar{G}^M_i = RT \ln a_i = RT \ln \gamma_i X_i \quad [7]$$

so

$$\gamma_{aq} < \gamma_{int}. \quad [8]$$

If the two regions are in fact in thermodynamic equilibrium, the activities in the interface region and in the bulk must be equal (Eq. [5]). In this case, the higher activity coefficient of the interface region requires that the concentration of metal ion be lower there than in the bulk aqueous solution. In this analysis, only the difference in permittivity of the two regions is considered; it does not account for other effects that may be operating at the interface, such as specific adsorption of ions.

If the interface is electrified the situation is a little more complicated. In this case the electrochemical potential, ζ, will be the same for all regions in thermodynamic equilibrium. In the bulk solution the electric field is assumed to be zero, so ζ reduces to μ, as defined in Eq. [4]. In an electrified region such as the surface, however,

$$\zeta_{int} = \mu^0 + RT \ln a_{int} + zF\psi_{int}, \quad [9]$$

where z is the charge on the ion, F is Faraday's constant, and ψ_{int} is the electric field strength at the surface. Setting the electrochemical potential at the surface equal to that in the bulk solution,

$$\mu^0 + RT \ln a_{aq} = \mu^0 + RT \ln a_{int} + zF\psi_{int} \quad [10]$$

$$a_{int} = \exp\left[\frac{RT \ln a_{aq} - zF\psi_{int}}{RT}\right]. \quad [11]$$

So, in the case of an electrified interface, the activity of a charged species differs from its value in the bulk.

According to the conceptual argument presented above, however, this change in activity cannot induce the formation of a neutrally charged precipitate. This is true because at a negatively charged interface the increase in the activity of the cationic component of a precipitate is exactly canceled out by the decrease in the activity of the anionic component, or vice versa for a positively charged interface. This result shows that surface precipitation cannot be caused by the disproportionate buildup of ions of a particular charge in the diffuse layer, as has been hypothesized (31). The argument

is illustrated for the case of $Co(OH)_2$, where $z_{Co^{2+}}$ is 2 and z_{OH^-} is -1, giving

$$a_{\text{int Co}^{2+}} \cdot (a_{\text{int OH}^-})^2 = \exp\left[\frac{RT \ln a_{Co^{2+}} - 2F\psi_{\text{int}}}{RT}\right] \times \exp\left[2\,\frac{RT \ln a_{OH^-} + F\psi_{\text{int}}}{RT}\right]$$

$$= \exp\left[\frac{RT \ln a_{Co^{2+}} - 2F\psi_{\text{int}}}{RT} + \frac{2RT \ln a_{OH^-} + 2F\psi_{\text{int}}}{RT}\right]$$

$$= \exp[(\ln a_{Co^{2+}} + \ln a_{OH^-}^2)]. \quad [12]$$

Hence,

$$a_{\text{int Co}^{2+}} \cdot (a_{\text{int OH}^-})^2 = a_{Co^{2+}} \cdot (a_{OH^-})^2 \quad [13]$$

and the surface does not cause oversaturation.

The consequence of this thermodynamic reasoning is that if precipitation is induced by the surface, it must be due to a reduction in the free energy of the solid phase. As pointed out above, there are at least two ways this could occur: (1) the precipitate, instead of being pure, could be coprecipitated with a component derived from the dissolved substrate, as in the model of Farley *et al.*, or (2) the total net change in the interfacial energies of the substrate and the precipitate could be negative.

In reality, substantial departures can occur from the behavior predicted by thermodynamic equilibrium. In general, kinetic factors can prevent a thermodynamically favored reaction from occurring, but cannot induce a thermodynamically forbidden transformation. As a result, the argument presented above constrains the conditions under which precipitation of a sorbate-bearing phase *cannot* occur, but not when it *will* occur. When reaction rates are extremely high, further deviations can take place. For example, sorbate ions could be trapped during rapid precipitation of another phase. However, the driving forces in our system should not be high enough to cause such anomalous effects.

The experiments in this study were designed to directly and conclusively show that surface precipitation can take place under conditions where the solution is undersaturated with respect to known bulk phases and to characterize any differences that may exist between the structures and morphologies of surface precipitates and bulk precipitates. Accordingly, samples of Co(II) were prepared under conditions that were both over- and undersaturated with respect to $Co(OH)_2(s)$, and these samples were characterized by a combination of methods that are sensitive to the differences in local atomic arrangements and microstructures that would be predicted by the different viable surface precipitation hypotheses. In addition, a sample of Co(II) coprecipitated with Al(III) was prepared for comparison with the sorption samples.

EXPERIMENTAL

Cleaning Procedure

In all the experiments presented here, the substrate used was Linde-A alumina powder from Praxair Corporation (formerly from Union Carbide). All experiments were done at room temperature, which ranged from 21 to 23°C. Two separate sets of uptake samples were studied, hereafter referred to as ''set 1'' and ''set 2.'' Different powder cleaning procedures were used for the two sets. For set 1, the method was designed to remove adsorbed anions and cations and proceeded as follows. Linde-A powder (10 g) and MilliQ DDI H_2O (40 ml) were put into Nalgene centrifuge tubes. After thorough mixing, the samples were centrifuged at $2000g$ relative force at room temperature for 30–50 min (this centrifuging procedure was used throughout the sample preparation), decanted, and refilled with DDI H_2O; this ''decanting process'' was repeated three times. The tubes were then titrated to pH 9 with NaOH and brought back to neutral by repeating the decanting process three times. The next step was to titrate the tubes to pH 4 with HNO_3; in this case four cycles of the decanting process raised the pH to 4.3. The powder was then filtered, and, after a 12-h interval, dried for 4 h at 70°C, and then stored in air in a glass vial.

The cleaning procedure used for set 2 was designed to remove a surface layer of $Al(OH)_3$ that could form on prolonged storage of the powder in a humid atmosphere. To do this, we relied on the fact that although $Al(OH)_3$ is more thermodynamically stable than Al_2O_3 in the presence of water, it also dissolves much more rapidly in hydrofluoric acid solution. Accordingly, 2 g of Linde-A powder were put into each of four 40-ml-capacity Nalgene centrifuge tubes, which were then filled with 1% HF, giving a pH of 2.2. These tubes were rotated end-over-end for 3 h. After centrifuging and decanting, 5 ml of DDI H_2O were added to each tube and then poured off without mixing up the paste at the bottom of the tube, and this cycle was repeated. The purpose of this step was to remove as many F^- ions as possible without shocking the pH. To remove the rest of the fluoride species, the paste was equilibrated 0.3 mM HNO_3 for 3 h, and then, after centrifuging, 95% of the supernatant was removed, replaced with water, and then mixed, and the cycle was repeated. After a total of four cycles (one being overnight), the pH had reached 5.1 in each tube. Finally, after two

TABLE 1
Summary of Solution Conditions for XAFS Samples

Set	Sample	Initial pH	Final pH	Initial concentration	Final concentration	Equilibration time
2	$\Gamma = 0.28$	4.98	8.10	153 μM	10.0 μM	160 h
1	$\Gamma = 0.30$	6.08	8.13	100 μM	10.3 μM	130 h
1	$\Gamma = 1.30$	5.53	8.16	1 mM	34 μM	130 h
2	$\Gamma = 1.59$	4.98	8.14	594 μM	5.4 μM	160 h
2	$\Gamma = 5.66$	5.08	8.10	2.2 mM	225 μM	140 h
2	$\Gamma = 23.1$	5.04	8.08	12.6 mM	2.17 mM	140 h
	Repeat 1	4.92	8.10	9.25 mM	1.16 mM	215 h
	Repeat 2	5.06	8.10	9.25 mM	1.21 mM	215 h

''decanting processes'' (as above for set 1), the powder was dried in an evacuated desiccator at room temperature and stored in air in a glass vial.

Uptake Experiments

Throughout this paper, for reasons of clarity the references to individual samples are made according to their final surface concentration in μmol/m^2, as measured by graphite furnace atomic adsorption spectroscopy (GFAA). All uptake experiments were conducted in an N_2 atmosphere to prevent contamination by carbonate. $Co(NO_3)_2$ solutions were prepared in concentrations ranging from 10^{-4} to 10^{-2} M by dissolution of reagent grade $Co(NO_3)_2 \cdot 6H_2O$ solid in sparged, MilliQ water, without any further additions to control the ionic strength (see Table 1 for a summary of the uptake conditions of each sample). To determine the initial Co concentrations, withheld aliquots of the solutions were analyzed using GFAA spectroscopy. Base titrations were conducted using small aliquots (1–100 μl) of CO_2-free NaOH, the concentration of which varied from 0.1 to 0.0001 N.

For set 1, two different solid-to-liquid ratios were used: 20 g/dm^3 for the $\Gamma = 0.30$ sample and 50 g/dm^3 for the $\Gamma = 1.30$ sample. The two samples were stirred for 24 h at the equilibrium pH of the mixtures. Over the next 5 days, the samples were titrated up to pH 8.1. During base additions, the tubes were stirred vigorously; the rest of the time, they were rotated end-over-end. In these titrations, as in all titrations in which powder was present, it was observed that the pH drifted slowly downward when the solutions were titrated up to pH 8. The very long titration times used were required in order to make the solution pH settle at 8.1.

After completion of the titration, the samples were centrifuged and aliquots of the supernatant reserved for analysis with GFAA. GFAA showed that both samples had uptake $\geqslant$90%. The pastes remaining in the tubes were loaded into Teflon XAFS sample holders and were sealed with Mylar tape. CoK edge XAFS data were collected within 2 days, in fluorescence mode using a 13-element Ge detector on beam line 4-2 at the Stanford Synchrotron Radiation Laboratory (SSRL). Multiple scans for each sample were collected in order to improve the signal-to-noise ratio. No TEM or XPS data were collected on the samples in set 1.

For each sample in set 2, 20 g/dm^3 of powder were placed in $Co(NO_3)_2$ solution in 40-ml polypropylene centrifuge tubes and titrated to pH 5. Base additions were made according to the same procedure used in set 1 and over a similar time span. For the highest coverage sample a set of two repeats was made in addition to the original sample, in order to test the reproducibility of the surface concentration measurements made with XPS and GFAA. At the end of the titration, the suspensions were centrifuged, and supernatant samples for GFAA analysis were removed with a polyethylene syringe and filtered with Teflon filters. The remainder of the supernatant was decanted and the solid split into two parts. One part was vacuum dried at room temperature and then stored in air, while the other was kept wet in sealed tubes under N_2. Blanks were conducted at the initial and final pH at solution concentrations of 50 and 1000 μM $Co(NO_3)_2$, in order to determine the amount of loss to the container walls. The concentrations of the blank solutions at various intermediate stages and at the final stage were determined with GFAA. Analysis of the solution concentrations showed that the fractional final uptake ranged from 83 to 99%, in all cases high enough that the signal from the solution phase could be safely ignored in the XAFS analysis. To summarize, the main differences between set 1 and set 2 are that all TEM and XPS analyses were done on set 2 and that set 2 was cleaned with HF while set 1 was not.

XPS data were collected from the dried portion of the samples in set 2, using a Fisons S-Probe spectrometer with Al$K\alpha$ X-rays and a 3-eV flood gun to achieve charge neutralization. TEM samples were prepared by putting a small drop of a highly dilute suspension of the equilibrated solid on a conducting foil and allowing the drop to dry under N_2, a process that took less than 5 min. The dilute suspensions were prepared in several ways: by diluting the contents of

a reaction tube before decanting, by resuspending a dry sample in a solution of the same pH and $Co(NO_3)_2$ concentration as the original supernatant, and by resuspending a dry sample in MilliQ H_2O. The differences among these methods had no apparent effect on the results. The TEM photos were taken with an Philips CM20FEG microscope operated at an electron energy of 200 keV. The XAFS samples were loaded and the data collected in the same fashion as for set 1, except that for set 2 the XAFS data collection took place 2 months later, using the wet paste from the sealed tubes. XAFS data were also collected on the dried portion of the $\Gamma = 1.59$ sample, to check if drying had a measurable effect on the local structure of the sorbate.

The EXAFS data from both sample sets were reduced with the EXAFSPAK programs (33), using phase and amplitude functions derived from model compounds ($Co(OH)_2$(s), $Co(NO_3)_2$(aq)) and from the FEFF 5.05 *ab initio* multiple-scattering codes (34–36). Final fitting was done on the normalized, background-subtracted raw data using all shells simultaneously. XANES data were analyzed by comparing sample spectra to calculations made using FEFF 6.01 (37). In these calculations, the AFOLP (automatic atomic overlap) card was used, and RMAX (maximum distance from the absorber in R-space) was set to 6.5 Å.

Coprecipitation Experiment

To test the possibility that sorption could take place via the formation of a ternary hydroxide of Co(II) and Al(III), we attempted to form a coprecipitate under solution conditions analogous to those present in the uptake samples, but without solid present. Based on work by Paces (38), the Al(III) concentration in pH 8.1 aqueous solution in contact with Linde-A powder is known to range from 0.5 to 5 μM, on the time scales of our sorption experiments. Accordingly, for the coprecipitation experiment, we prepared 500 ml of 2 μM $Al(NO_3)_3$ solution with ionic strength of 0.1 M (from $NaNO_3$) in a 1000-ml HDPE beaker that had been preequilibrated with Al(III) solution to prevent container losses. In a separate beaker, we prepared 500 ml of 250 μM $Co(NO_3)_2$ solution at the same ionic strength (this concentration is 80% of the value required to precipitate $Co(OH)_2$ at this pH). Each of these solutions was separately titrated to pH 8.10, at which time light scattering from a HeNe laser showed that no precipitates were present in either solution. The Co(II) solution was then added to the Al(III) solution, with pH being monitored. A pH change from 8.10 to 8.05 was observed, and light scattering showed that a colloid had formed. Over the next 24 h, the pH of the stirred suspension decreased to 7.93. At the end of this period, the suspension was vacuum filtered using a 0.1-μm polycarbonate filter. XAFS spectra were collected from the reserved filter membrane under conditions similar to those of the sorption samples.

RESULTS

Adsorbent

We chose to use Linde-A alumina powder as the sorbent in this study because it has been used in several past studies (2, 3, 39, 40) and as a result the surface properties have been extensively characterized. According to this past work, the surface area, as measured by N_2-BET, is 15 m^2/g (41) and the pH_{PZNPC} (point of zero net proton charge) has a value of 8.9 (40). However, subsequent TEM analysis, plus inquiries to the manufacturer, revealed that it is composed of about 90% α-Al_2O_3 and 10% γ-Al_2O_3, which was not revealed in powder XRD scans due to the small particle size and poor crystallinity of the γ-Al_2O_3 grains. According to the manufacturer, the powder has less than 0.5 wt% H_2O (a value consistent with sorption of water from ambient air), leading us to believe that no $Al(OH)_3$ is present in the as-delivered material.

TEM photos of the as-delivered powder (see Fig. 3) showed that there are two distinct powder particle morphologies, clumped in separate regions. Electron diffraction patterns of the larger particles indicate that they are made up of highly crystalline α-Al_2O_3. The grains are prolate ellipsoidal in shape, with the longer dimension ranging in size from approximately 100 to 500 nm. Electron diffraction showed that the smaller particles are predominantly γ-Al_2O_3, with wide rings indicating that the material has poor crystallinity. The γ-Al_2O_3 grains do not have any characteristic shape and range in size from about 10 to 30 nm. From the micrographs, it was possible to determine upper and lower bounds for the volume fractions of the two morphologies: 70% α-Al_2O_3/30% γ-Al_2O_3 and 97%/3%. These bounds are consistent with the 90%/10% phase distribution reported by Praxair. From the TEM photos, the average dimensions of the α-Al_2O_3 and γ-Al_2O_3 particles were calculated to be 230 and 17 nm, respectively. Assuming that each phase is composed of spheres with these characteristic dimensions and that the actual volume fractions of α- and γ-Al_2O_3 are 90/10, the relative surface areas of the two phases were calculated to be about 40% α-Al_2O_3 and 60% γ-Al_2O_3.

While a heterogeneous substrate can complicate analysis of sorption samples, it does not turn out to have serious consequences for the purposes of this study. If the XAFS results were being used to try to determine the structure of adsorbed complexes, the heterogeneous substrate would present a greater problem, as the difference in coordination of Al in the two substrates (octahedral only in α-Al_2O_3, but both octahedral and tetrahedral in γ-Al_2O_3) would make data analysis more complicated. The exact nature of these polyhedral linkages, however, has little effect on the interpretations of the XAFS in the present study. The heterogeneous substrate does not confuse the interpretation of the

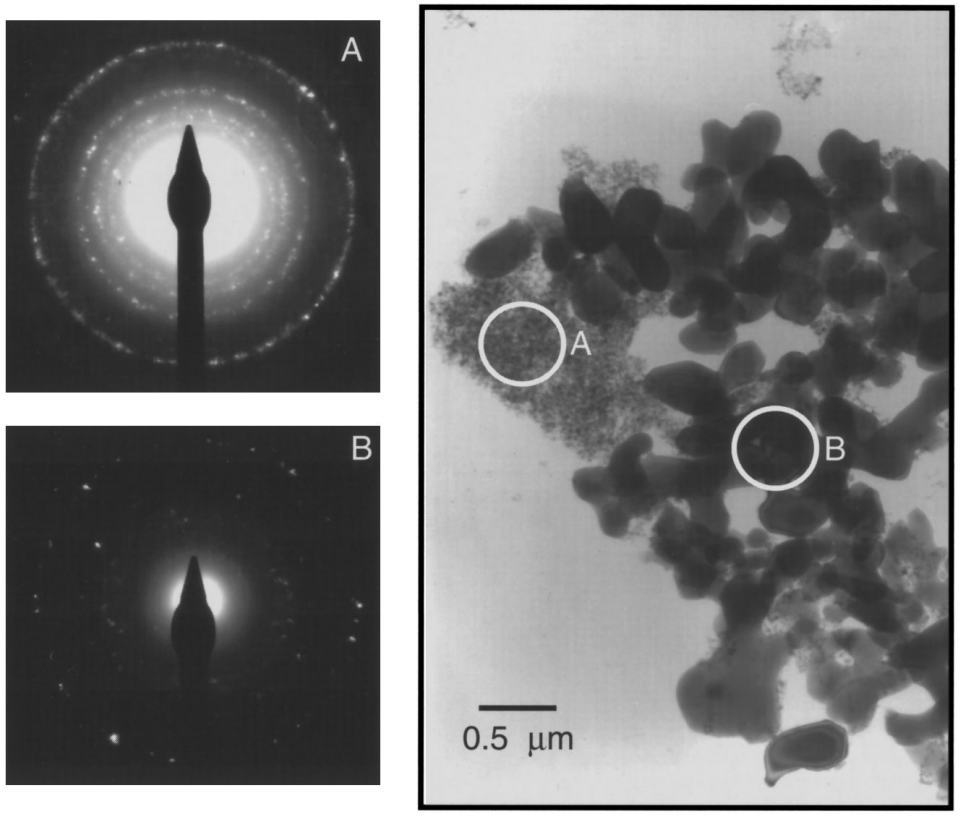

FIG. 3. Representative TEM image of Linde-A alumina. The electron diffraction patterns show that the regions with smaller grains consist mainly of γ-Al_2O_3, (A), while the larger grains consist of α-Al_2O_3 (B). The diffraction pattern shown for α-Al_2O_3 was measured from a larger region with many more grains present than in the image shown.

TEM images, because the images themselves show the way in which the Co clusters are associated with the two alumina phases. There is, however, one aspect that must be considered—the difference in the solubilities of the different alumina phases present. Transition aluminas such as γ-Al_2O_3 dissolve more readily than α-Al_2O_3, leading to a higher Al concentration in solution and hence to a greater likelihood of coprecipitation.

The cleaned powder of set 2 was also characterized with XPS and TEM. The only surface contamination detected by XPS was approximately 2 at.% of fluorine in the surface region, from the HF cleaning step. Low-resolution TEM showed no change from the as-delivered material. Evidence from FTIR spectroscopy (Per Persson, unpublished data) has indicated that aluminum hydroxide, most likely bayerite, forms on prolonged exposure of α-Al_2O_3 to water. To determine whether $Al(OH)_3$ might have formed, the cleaned powder was examined with high-resolution TEM. The phase identity of particular particles could be constrained by measuring the fringe spacing in these images. This method indicated that other transition aluminas (notably θ-Al_2O_3) were intermixed with the γ-Al_2O_3, though as a small fraction. There was no evidence from TEM fringe-spacing measurements for the presence of any hydroxide phases. The TEM, however, would not be sensitive to coatings of a hydroxide phase whose thickness is a just few monolayers.

After the sorption of Co(II), the phase composition of the substrates was again examined in detail with TEM. The micrographs (not shown) indeed indicate the presence of particles of an Al-hydroxide phase, though the fringe-spacing measurements cannot be made with sufficient precision to distinguish among several forms of $Al(OH)_3$ with similar structures. In order to judge how much effect the formation of a hydroxide phase might have on the surface properties, we calculated the maximum amount of Al_2O_3 that may have dissolved during the time span of the experiment. Using data for the rate of dissolution of δ-Al_2O_3 at pH 3 (42), we found that a maximum of 0.5% of the Al_2O_3 could have dissolved, which should be a very conservative upper bound as Al_2O_3 is much less soluble under the pH conditions of our experiments. Since the reprecipitated $Al(OH)_3$ is present as distinct grains, and because in very few cases was there any evidence for coatings being formed, it seems likely that a negligible fraction of the total surface area is made up of $Al(OH)_3$.

TABLE 2
Comparison of Surface Concentrations Calculated from XPS and from GFAA Data

Sample	GFAA[a]	XPS[a]
$\Gamma = 0.28$	0.28	0.32
$\Gamma = 1.59$	1.59	1.08
$\Gamma = 5.66$	5.66	3.60
$\Gamma = 23.1$	23.1	11.9
Repeat 1	25.1	11.8
Repeat 2	25.0	13.2

[a] In μmol/m^2.

Sorbate

A comparison of the sorption density information as measured by XPS and by N_2-BET and GFAA is presented in Table 2 and Fig. 4. To calculate the XPS surface coverage, the escape depth of electrons in Al_2O_3 (43) was used to find the areal density of Al atoms that would be seen with no adsorbed Co. Based on the Al 2*p* and Co 2*p* peak areas and cross sections, the areal density of Co atoms could then be calculated. The same calculation was made assuming that a uniform Co-bearing overlayer absorbed the photoelectrons, but the correction was negligible even at the highest sorption density. In this calculation the electron escape depth was calculated empirically (44), assuming the overlayer to have the properties of $Co(OH)_2$.

As the sorption density increases, the sorption density measurement by XPS underpredicts that by GFAA by progressively greater amounts. This discrepancy suggests that, except in the sample with the lowest sorption density, the Co ions are grouped in clusters that are sufficiently large to occlude the signal from the inner Co atoms, while much of the Al_2O_3 surface is left bare. This conclusion is corroborated by evidence from the TEM photos, where plate-like precipitates were seen in samples with high or intermediate sorption density ($\geq$1.59 μmol/m^2), but not in the one with lowest sorption density (0.28 μmol/m^2).

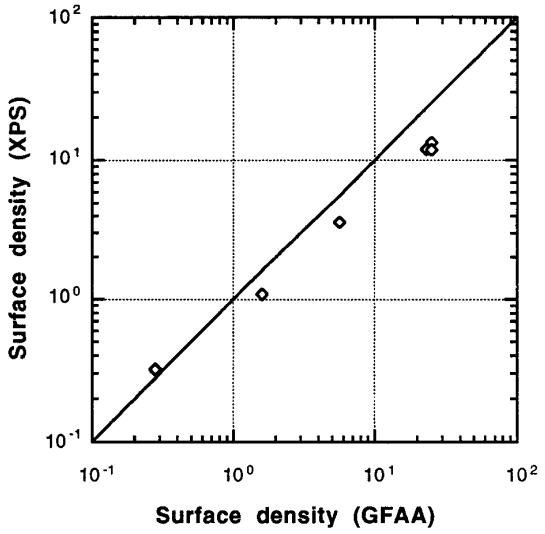

FIG. 4. Comparison of the surface concentration of Co on Al_2O_3 from XPS and GFAA measurements. Three repeats were done of the highest coverage sample. The solid line shows where the two techniques give the same result. The ''missing Co'' in the XPS measurements at the highest coverage indicates that the Co-bearing precipitates are large enough that they occlude the Co signal more than the Al signal.

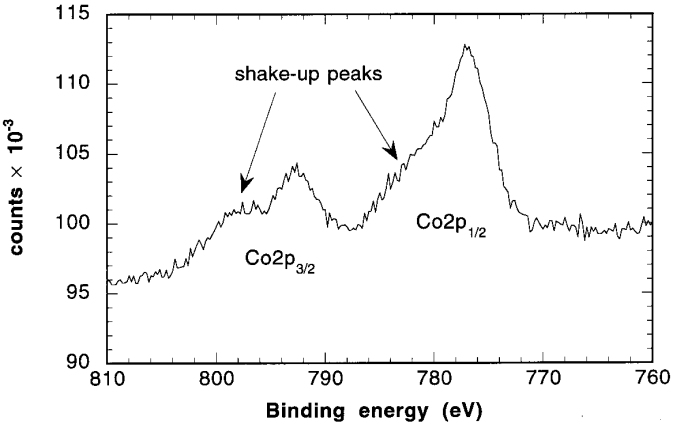

FIG. 5. XPS spectrum of Co2$p_{1/2}$–2$p_{3/2}$ from sample Γ = 23.1. The satellite structure is characteristic of high spin Co(II).

The oxidation and spin state of the Co atoms can be identified from the shape of the Co 2*p* lines (Fig. 5). The satellite structure on the high binding energy side of the principal 2$p_{1/2}$ and 2$p_{3/2}$ lines is characteristic of high spin Co^{2+} (45). Due to broad spectral lines and problems with sample charging, the shakeup peak is a more easily identified characteristic of the chemical state of the Co than either the absolute binding energy or the 2$p_{1/2}$-2$p_{3/2}$ line separation.

Results of the XAFS analysis of the six samples, as well as data from X-ray diffraction on the local structure around Co in $Co(OH)_2$ (14), are presented in Table 3. The EXAFS and their corresponding Fourier transforms are shown in Fig. 6. For each of the sorption samples, the distance to the first-nearest-neighbor oxygen atoms is 2.08 ($\pm$0.01) Å. This distance is consistent with other EXAFS measurements made on Co sorption samples and solution complexes (17, 29) but slightly smaller than the Co–O distance in $Co(OH)_2$(s) (2.10 Å). The oxygen neighbors may be from oxygen ions, hydroxyl ions, or water molecules; EXAFS is unable to distinguish among these possibilities since hydrogen atoms are too light to cause measurable backscattering. In the initial fitting of the data, the number of O neighbors was allowed to vary. Since in each case this number was within 10% (the expected error (46)) of 6, the coordination number that is expected for Co in this chemical environment, the number of O neighbors was fixed at 6 in all of the final

TABLE 3
Quantitative EXAFS Fitting Results

Set	Sample	N_O[a]	σ^2_O[b]	R_O[c]	N_{Co1}	σ^2_{Co1}[b]	R_{Co1}[c]	N_{Co2}	σ^2_{Co2}[g]	R_{Co2}[c]
2	$\Gamma = 0.28$	6	0.0053	2.09	0.6	−0.0015[b]	3.12	[e]	[e]	[e]
1	$\Gamma = 0.30$	6	0.0044	2.09	0.9	0.0017	3.11	[e]	[e]	[e]
1	$\Gamma = 1.30$	6	0.0044	2.09	2.5	0.0044	3.10	2.5	0.0044	6.14
2	$\Gamma = 1.59$ (wet)	6	0.0028	2.08	3.2	0.0045	3.07	4.1	0.0045	6.10
2	$\Gamma = 1.59$ (dry)	6	0.0024	2.08	3.0	0.0056	3.09	3.4	0.0056	6.14
2	$\Gamma = 5.66$	6	0.0036	2.09	3.3	0.0035	3.10	3.3	0.0035	6.16
2	$\Gamma = 23.1$	6	0.0071	2.07	4.0	0.0078	3.10	3.0	0.0078	6.18
	$Co(OH)_2$[f]	6	0.004[b]	2.10	6	0.004[b]	3.17	6	0.004[b]	6.34
		N_O[a]	σ^2_O[b]	R_O[c]	N_{Co}[d]	σ^2_{Co}[h]	R_{Co}[c]	N_{A1}[d]	σ^2_{A1}[h]	R_{Co}[c]
	Co-Al ppt	6	0.0055	2.09	3.36	0.005	3.09	2.64	0.005	3.04

[a] When allowed to float, N_O was within 10% of 6 for all the samples in this study (allowing for self-absorption in the $\Gamma = 23.1$ sample). Since there is reason to believe that the Co is 6 coordinated, N_O has been fixed at 6 to reduce the number of fitting parameters.

[b] In Å^2. These shells are fitted using $Co(OH)_2$ as a model. Errors in the assumed values of σ^2(0.004 Å^2 in each case) for $Co(OH)_2$ will propagate as errors in the fitted σ^2 values, and can result in anomalously low fitted values.

[c] In Å.

[d] Due to amplitude cancellation between the Co and Al shells, the number of second neighbors is poorly constrained. Consequently, the total number of second neighbors (Co and A1) has been set to 6.

[e] There was little or no contribution from this shell in these samples.

[f] N and R values from X-ray diffraction (14).

[g] In Å^2.σ^2_{Co2} values were constrained to be the same as σ^2_{Co1} in order to reduce the number of fitted parameters.

[h] The Debye-Waller factor was fixed at 0.005 Å^2 for these shells.

fits. For the sample with the highest sorption density, the XAFS were attenuated and the sharp features were less well resolved, an effect that we attribute to self-absorption of the incident X-rays. To correct for the self-absorption, the procedure prescribed by Tröger *et al.* (47) was applied.

The radial distance from the absorber to the second-neighbor cobalt atoms is 3.10 (±0.02) Å for each of the samples. This distance is consistent with adjacent CoO_6 octahedra sharing edges, the arrangement found in $Co(OH)_2$. However, it is somewhat smaller than the Co–Co distance seen in $Co(OH)_2$ (3.17 Å), even when the difference in the Co–O distance is taken into consideration. The smaller distance suggests that the octahedra in the sorption complexes are less distorted than those in $Co(OH)_2$, where they are flattened along a threefold axis.

Figure 6 also shows a FEFF-generated simulation of the EXAFS and Fourier transform of a Co atom sitting on an Al lattice site in the α-Al_2O_3 structure. Some distortion of the oxygen first shell has been included in order to better accommodate the Co ion in the smaller Al octahedral site. It can be readily seen that none of the second-neighbor peaks correspond to those found in the data. Thus, we can reject the possibility that the Co has been incorporated into the α-Al_2O_3 matrix. Further, since for a surface Al-equivalent site the peak positions would be largely unchanged even though their amplitudes would be reduced, we can also reject the hypothesis that a Co adsorbs at such a site. A similar analysis of Co substitution for Al in the γ-Al_2O_3 structure shows that this possibility is also excluded.

In addition to the fitting information for the uptake samples, Table 3 shows the results from EXAFS analysis of the dried portion of the $\Gamma = 1.59$ sample. As the fitted parameters show and Fig. 6(b) confirms, the EXAFS spectra from the wet and dry samples are essentially identical. This similarity indicates that it is safe to extrapolate the data collected on dry samples (e.g., using TEM or XPS) to the case where bulk water is present on the surface. Of course, this conclusion is based on just one sample and may be applied only to the drying procedure used in this study. In fact, in another sample (not shown here) where the paste was air-dried at room temperature, the X-ray absorption near-edge structure (XANES) was markedly different from the *in situ* case.

The XANES spectrum of the $\Gamma = 23.1$ sample is shown in Fig. 7. The XANES of the samples with lower surface concentration are similar, though for these samples there is no amplitude reduction due to self-absorption. Despite the general similarities between the EXAFS of this sample and that of $Co(OH)_2$(s), the XANES spectra are markedly different. Unlike the EXAFS portion of the X-ray absorption spectrum, which is primarily sensitive to single scattering, the XANES is extremely sensitive to multiple scattering among first, second, and more distant oxygen neighbors. This difference is a consequence of several factors that act at low electron momentum (k), including less amplitude reduction by high Debye-Waller

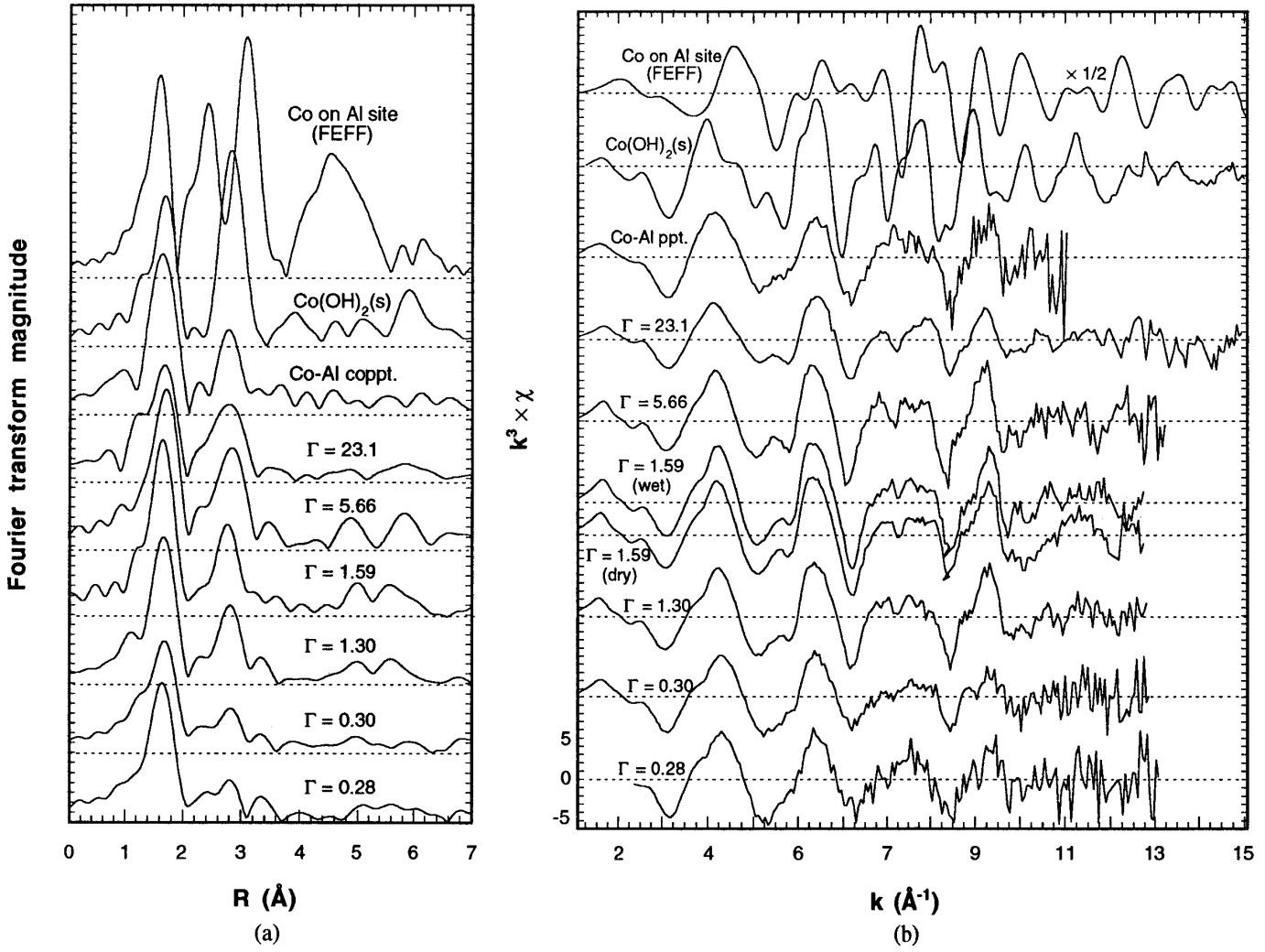

FIG. 6. EXAFS and Fourier transforms (uncorrected for phase shift, Δ) of samples, $Co(OH)_2$ solid model, and a FEFF-generated model of Co occupying an Al lattice site in α-Al_2O_3. Also shown in (b) is a comparison of the EXAFS of sample $\Gamma = 1.59$ collected as a wet paste (''wet'') and as a vacuum-dried powder (''dry'').

factors, higher scattering probability at angles away from 0° and 180°, and the high amplitude for oxygen backscattering in this region of k space. Since these effects have significant contributions out to about $k \leqslant 5$ Å^{-1} for these spectra, the XANES analyses have been extended somewhat further from the absorption edge than is commonly the case. The differences in XANES spectra indicate that the extended oxygen environment around Co differs significantly in the precipitate sample and in the solid model.

Figures 6 and 7 also show the EXAFS spectrum, Fourier transform, and XANES spectrum of the Co(II)–Al(III) coprecipitate. In general, the coprecipitate spectra are similar to the sorption sample spectra of intermediate surface coverage ($\Gamma = 1.30$–5.66 μmol/m^2) and do not resemble the $Co(OH)_2$ spectra. Unlike the sorption samples, however, the EXAFS of the coprecipitate can be fit adequately only if Al as well as Co is included in the second shell. The most plausible fit values for N and R are shown in Table 3. However, due to the inherent uncertainty in fitting multiple second shells to data of this quality, these ''best'' fit values should not be considered the only possibilities.

The TEMs of the sorption samples show the presence of plate-shaped precipitates. A notable exception to this is the lowest sorption density ($\Gamma = 0.28$) sample, where no precipitates were found. Energy dispersive spectroscopy (EDS) revealed that the Co is inhomogeneously distributed throughout the matrix in both α- and γ-Al_2O_3 and that the precipitates contain Co but little Al (Fig. 8). Since the electron beam penetrates the entire thickness of the sample, it is unclear whether the Al signal which appears to come from the precipitate (Fig. 8b) is due to the precipitate or to Al_2O_3 matrix that is either above or below it. The majority of these Co-containing

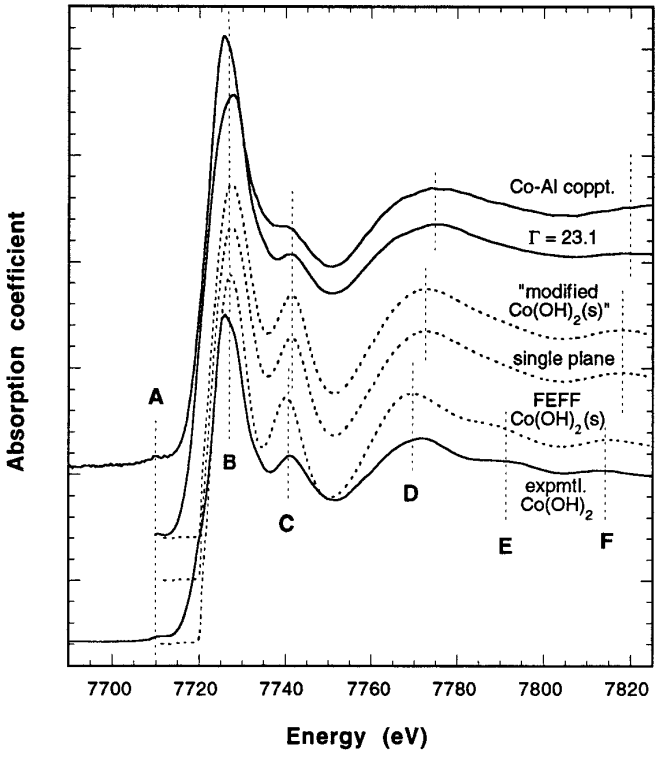

FIG. 7. Co K-XANES spectra of the Co(II)–Al(III) coprecipitate, the $\Gamma = 23.1$ sample, $Co(OH)_2(s)$, and comparison to calculations using FEFF 6.01. Though the amplitudes are not perfectly matched, the FEFF calculations are able to successfully model the presence and positions of features B–F.

precipitates seem to be associated with the γ-Al_2O_3 regions. Lattice images of the Co-bearing phase in the $\Gamma = 23.1$ sample indicate that it consists of poorly crystalline grains of $Co(OH)_2(s)$, with numerous extended defects and areas that exhibit little or no diffraction (Fig. 9). There is no evidence for an epitaxial relationship between the precipitates and the Al_2O_3 grains, though in a few cases $Co(OH)_2(s)$ precipitates in immediate contact with α-Al_2O_3 surfaces were observed. At decreasing Co sorption density, fewer and smaller $Co(OH)_2$ precipitates were seen, but in all cases the distribution of plate thicknesses seems to follow a skewed distribution, with the minimum size (2.4 nm) being about half the mean size (4.6 nm) (Fig. 10). For all but the highest sorption density sample ($\Gamma = 23.1$), the supernatant solutions were undersaturated with respect to $Co(OH)_2(s)$ (see Fig. 11).

DISCUSSION

Data Interpretation

XAFS data from the sample with highest sorption density provide information about the structure and morphology of the surface precipitate phase. At this sorption density, there is reason to believe that virtually all the cobalt is present in the form of a precipitate rather than as an adsorbate, since (a) the sorption density is so high, at 23.1 μmol/m^2, that if it were adsorbed several monolayers would need to be present; (b) the XAFS are quite similar to that of solid $Co(OH)_2$, even including the characteristic feature at 5.5 Å in the Fourier transform (not corrected for phase shift) which is due to multiple scattering among linearly arranged Co atoms (29); and (c) the XAFS is nearly the same as for Co/SiO_2 (1) and for the higher sorption densities of Co/kaolinite (48), which would be a surprising result except in the case of a precipitate.

The combined XAFS and TEM results give a fairly clear picture of the structure of this precipitate and its relationship to the Al_2O_3 matrix. In the $\Gamma = 23.1$ sample, the EXAFS is similar to that of $Co(OH)_2(s)$, but it also differs in various respects. Most significantly, the distance to each of the shells is distinguishably different from $Co(OH)_2(s)$: the Co–O distance is 2.07 Å vs 2.10 Å, the Co–Co second-neighbor distance is 3.10 Å vs 3.17 Å, and the longer Co–Co distance (>6 Å) is 6.18 Å vs 6.34 Å (in both cases twice the closer Co–Co distance) (Table 3). Also, there are fewer second neighbors in the sorption sample, 4 vs 6 in $Co(OH)_2$. These differences are consistent, we believe, with a $Co(OH)_2$-like precipitate phase which is hydrous and highly disordered, with a structure as illustrated in Fig. 12. According to this hypothesis, such a solid would have a structure analogous to that of $Co(OH)_2$, with each Co having six nearest oxygen neighbors, but with numerous Co vacancies. Based on the coprecipitation data, it seems likely that some Al is present in the coprecipitate, although no Al backscattering can be detected in the XAFS. The Co vacancies would be charge-compensated by Al, and perhaps also by substitution of H_2O for OH^-; neutron diffraction work suggesting that H_2O can substitute for OH^- in high-surface-area $Ni(OH)_2$ (49) indicates that such a substitution is possible. The hypothesis of a hydrous, disordered $Co(OH)_2(s)$-like precipitate is corroborated by the high-resolution TEM, which shows that the precipitates are highly defected, having curved basal planes, extended defects, and regions so disordered that they do not produce diffraction fringes (Fig. 9).

The difference between the Co–Co distance we observed and that found in crystalline $Co(OH)_2(s)$ (0.07 Å) is consistent with an earlier powder X-ray diffraction study (50) in which α-$Ni(OH)_2$ was found to have *a* and *b* unit cell dimensions that are 0.05 to 0.1 Å smaller than in β-$Ni(OH)_2$. These two forms of $Ni(OH)_2$ correspond to the α- (blue) and β- (pink) forms of $Co(OH)_2$, respectively. A subsequent study, however, attributed this apparent shortening to a systematic error in the analysis of the diffraction data (51). In spite of this diffraction result, the EXAFS results indicate a true shortening of the Co–Co distance in the sorption samples relative to that in β-$Co(OH)_2$. Given the close analogy between the structures and properties of

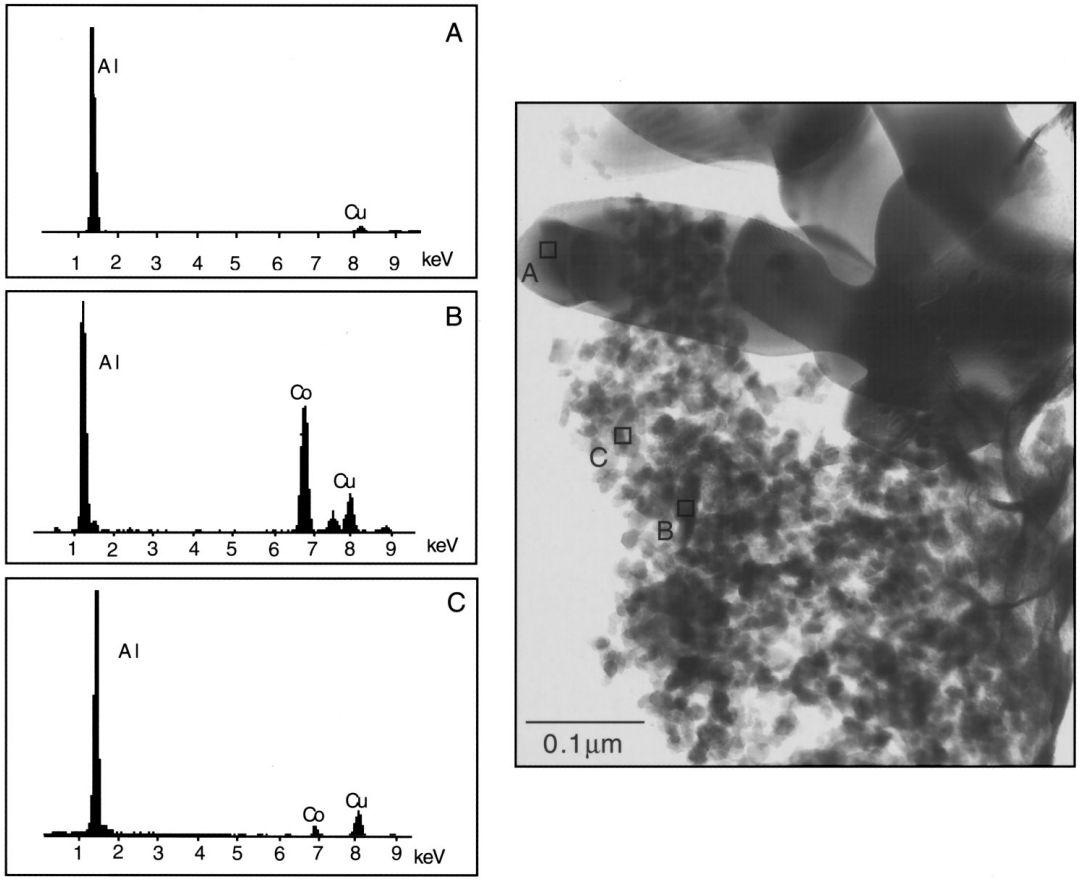

FIG. 8. Representative EDS spectra from various regions of the $\Gamma = 1.59$ sample. In general a varying amount of Co is found in both the α-Al_2O_3 and γ-Al_2O_3 regions (as shown by the representative spectra shown for spots A and C). Some Al signal is seen when the electron beam is placed on a precipitate particle (B). This signal may come from Al_2O_3 matrix lying above or below the position of the precipitate grain or from the precipitate itself. The samples are supported on a copper grid, which gives rise to the copper signal seen in all spectra. The small peak at 7650 eV (between the Co and Cu peaks) in (B) is due to CoK_β fluorescence.

$Ni(OH)_2$ and $Co(OH)_2$, one possible explanation for our XAFS results is that the surface precipitates consist of α-$Co(OH)_2$. In fact, it has been suggested that the structure of α-$Ni(OH)_2$ is hydrous and disordered, similar to the structure we propose for the surface precipitates. On the other hand, both the blue form and the pink forms of $Co(OH)_2(s)$ have been shown to have the same XAFS (29), though it is hard to be sure how much of the blue $Co(OH)_2$ might have converted to pink during the course of those XAFS measurements.

The local structure of the surface precipitate can be constrained still further by comparison of the Co*K*-XANES of this material with that of $Co(OH)_2(s)$ and to theoretical calculations of the XANES spectra using the FEFF 6.01 multiple scattering code. As may be seen in Fig. 7, by using a sufficiently large fragment of the $Co(OH)_2(s)$ structure centered at the Co absorber (out to 6.35 Å, including all O atoms), FEFF is able to reproduce accurately the positions of features in the XANES spectrum of $Co(OH)_2$. Neither the theoretical calculations nor the experimental data for $Co(OH)_2(s)$ accurately reproduce the XANES observed for the surface precipitates. In particular, the feature marked E in the spectrum from $Co(OH)_2$ is missing in the $\Gamma = 23.1$ spectrum, and the positions of features C, D, and F are substantially shifted. FEFF 6.0 calculations reveal that the XANES spectra come about as the result of the superposition of contributions from many different low amplitude oxygen multiple scattering paths. The particular details of the $Co(OH)_2(s)$ spectrum result from contributions of paths including O atoms both in the same Co–O octahedral layer as the absorbing Co and in the adjacent layers. However, fairly small shifts in the oxygen positions significantly reduce the contribution of paths which include oxygens outside the octahedral layer. As a result, the XANES spectra do not allow us to distinguish between models in which the precipitate structure is only slightly distorted compared to β-$Co(OH)_2$ and models in which the neighboring layers have no crystallographic relationship to one another. This is

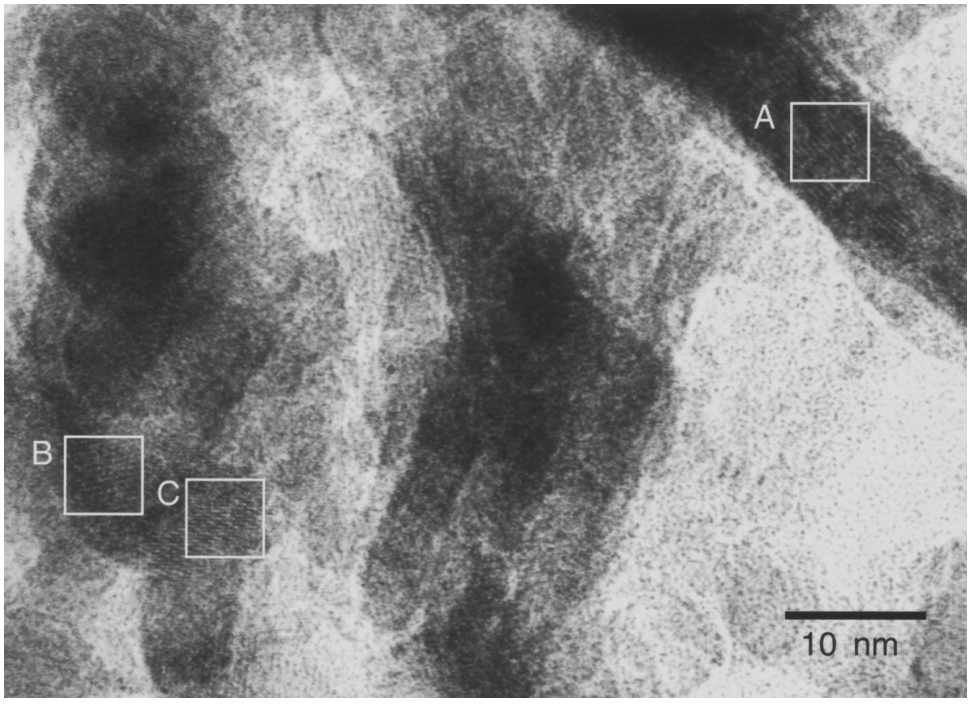

FIG. 9. High-resolution TEM image of a precipitate particle surrounded by γ-Al_2O_3 matrix. The square labeled A shows an area where diffraction fringes from the precipitate may be observed; the fringe spacing (about 4.7 Å) corresponds to the (001) plane spacing of β-$Co(OH)_2$ (4.64 Å). The regions labeled B and C have fringe spacings of 4.5 and 2.7 Å, corresponding to the (111) plane spacing of γ-Al_2O_3 and the (202) plane spacing of θ-Al_2O_3, respectively.

illustrated in Fig. 7, in which two models are shown for the precipitate XANES spectrum, one being a distorted β-$Co(OH)_2$ structure (the extent of distortion being based on the EXAFS data), the other being an isolated distorted basal plane. The XANES calculations confirm, however, that the model we propose for the structure of the individual octahedral layers—hexagonally closest packed CoO_6 octahedra, slightly reduced in size and less flattened than in $Co(OH)_2$(s)—accurately describes the structure found in the surface precipitate.

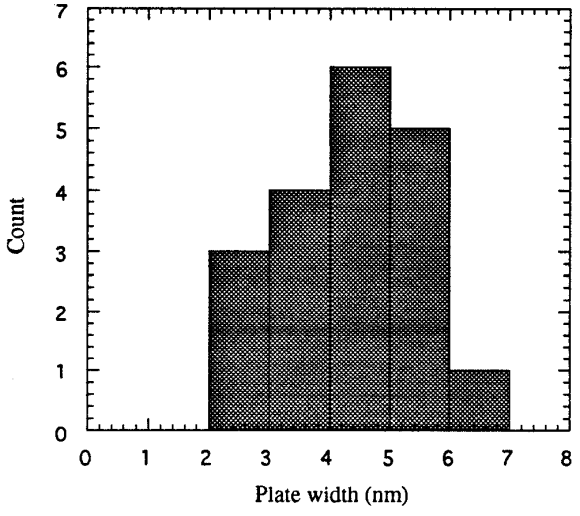

FIG. 10. Histogram of the plate thickness of precipitate particles in Γ = 1.59 sample, from TEM.

In the lowest surface concentration sample (Γ = 0.28) no precipitates were seen with TEM, but the EXAFS analysis revealed the presence of second-neighbor Co atoms at the same distance as seen in the higher sorption density samples (3.10 Å). There are two possible explanations for this observation: either Co multinuclear complexes form at the surface under conditions where no precipitates are present and essentially no multinuclear complexes exist in solution or precipitates were in fact present but were either so few or were sufficiently different in morphology from those seen at higher surface concentrations that they could not be observed by TEM. Although there is no simple quantitative means of determining the true lower limit of detection of precipitates with TEM, the first of the two explanations seems most likely. It would be remarkable if no precipitates were observed had they actually been present, given that many different areas of the sample were examined and that they were so obvious in the higher concentration samples. Furthermore, comparison of the XPS and GFAA data is consistent with precipitates being present in the higher concentration samples but not in the Γ = 0.28 sample, since in this sample XPS results did not underpredict the sorption density measured by GFAA and N_2-BET.

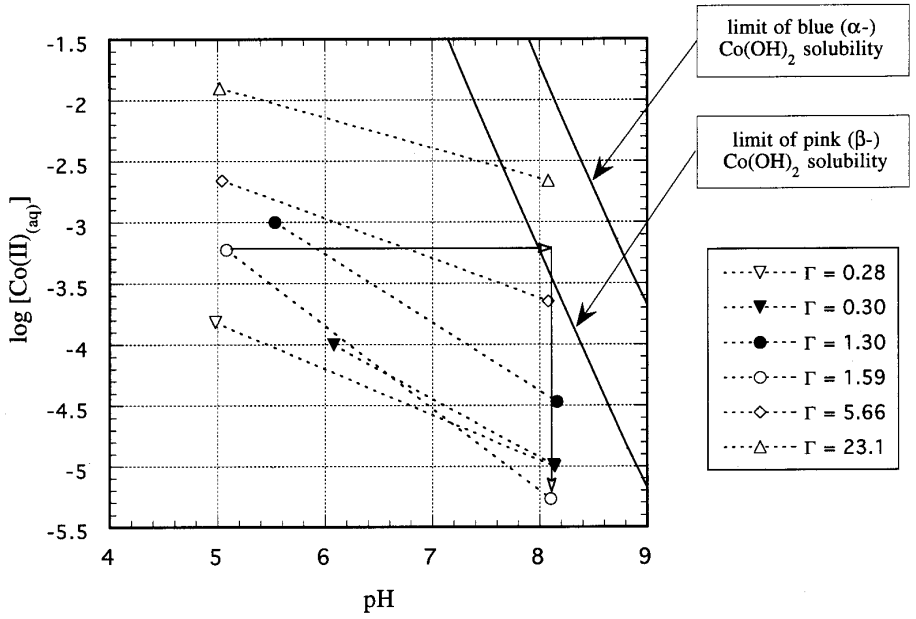

FIG. 11. Initial and final pH values for the XAFS samples, with comparison to the saturation concentrations of blue (metastable) and pink (stable) $Co(OH)_2(s)$. The arrows show the path through pH concentration space that would be followed if no sorption took place, that is, the path that would result in the most saturated conditions possible. In practice, if any sorption took place at a pH lower than 8.1, the actual path would fall below and to the left of the arrows.

In previous XAFS work on similar systems which were not examined by TEM, it has not been possible to distinguish between multimeric complexes and mixtures of multimeric complexes, precipitates, and/or monomers. As a result, it was impossible to determine if a true multimeric sorption regime existed (as has been proposed by several workers (3, 52, 53)), or if sorption shifted directly from monomeric adsorption to precipitation (as has been suggested by others (23)). The small number of Co second-neighbors found from the EXAFS analysis (about 1) indicates that the complexes seen in $\Gamma = 0.28$ sample are either predominantly dimeric or made up of a mixture of monomers and small oligomeric species. Dimeric ($Co_2(OH)^{3+}$) and tetrameric ($Co_4(OH)_4^{4+}$) complexes have been postulated to exist as solution species (20), though not at the pH and metal ion concentrations prevailing for these samples. These polymeric complexes, though, are of a size consistent with our EXAFS results. Structurally, the Co coordination environment in the polymers must be similar to that in $Co(OH)_2(s)$ (i.e., they are made up of edge-shared octahedra), the only significant differences being the smaller Co–Co interatomic distance (a difference of 0.05 Å) and the smaller Debye-Waller factor (0.006 $Å^2$ difference) seen here as compared to $Co(OH)_2(s)$.

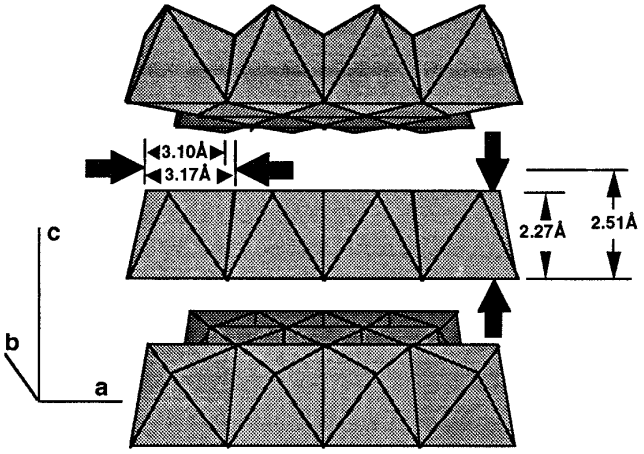

FIG. 12. Polyhedral representation of the structure of $Co(OH)_2(s)$. The arrows indicate the differences between the $Co(OH)_2(s)$ structure and the ''modified $Co(OH)_2(s)$'' structure.

Constraints on Surface Precipitation Models

In Fig. 11 it may be seen that none of the samples was at any time oversaturated with respect to the active blue (α) form of $Co(OH)_2$, which precipitates before the pink (β) form of $Co(OH)_2$. Furthermore, since the conditions at which the samples stabilized were all at the same pH but different final solution concentrations, it may be conclusively said that precipitation of bulk $Co(OH)_2$ is not controlling the amount of uptake. However, since the Co solution concentration is measured only at the beginning and end of the uptake reaction, it is not known what path through pH–

concentration space the reaction actually followed. Thus, the solution may have passed through the region of oversaturation, especially in the case of the two most concentrated samples.

For the $\Gamma = 1.59$ sample, however, the TEM shows the presence of precipitates even though the supernatant was never oversaturated with respect to blue $Co(OH)_2(s)$, even assuming that no adsorption took place (i.e., the path through pH–concentration space is right-angled, as illustrated in Fig. 11). Insofar as any uptake occurs at a pH less than 8.1, the actual reaction path would lie below the right-angle path; as a result, it seems likely that this sample was never oversaturated with respect to pink $Co(OH)_2(s)$, either. Even for the $\Gamma = 5.66$ sample, some explanation other than $Co(OH)_2(s)$ precipitation must be found for the fact that the final solution concentration is a factor of 2 below the saturation of the most stable (pink) $Co(OH)_2$ phase. In short, there is clear evidence that surface precipitation, as defined at the beginning of the paper, has occurred in this system.

Two lines of reasoning lead us to believe that the surface precipitation we observe in the $Co(II)/Al_2O_3$ system comes about as a result of the formation of a ternary (or double) hydroxide phase. First, we have not been able to propose any other model that can account for the XAFS, TEM, XPS, and solution behavior. Second, using solution conditions similar to those used in the sorption experiments, we have produced a Co(II)–Al(III) basic coprecipitate whose structure closely resembles that found for the surface precipitates. Before considering these two arguments, however, it is worth examining other factors that might explain the observation of precipitation from an undersaturated solution.

(1) The thermodynamic data for the solubility of $Co(OH)_2$ could be incorrect. This seems unlikely since in the solubility measurements (14, 15) equilibrium was approached from both the undersaturated and the oversaturated directions, to control for kinetic effects. Furthermore, for both the blue and pink forms of $Co(OH)_2$, the solubility values have been determined independently by different groups and were found to be nearly identical.

(2) Precipitation may proceed much faster than adsorption. This would allow the right-angle path to be followed in the pH–concentration diagram (Fig. 11), and then the slower adsorption process could continue to lower the concentration even after the solution is no longer saturated with respect to the precipitate. This explanation could apply even to the lower sorption density samples if the pH was overshot during the titration. If this dissolution and subsequent adsorption mechanism were correct, dissolution of the precipitate must be kinetically inhibited even though its formation is kinetically favored. This explanation is unsatisfactory, however, because the rates it implies (precipitation proceeding faster than adsorption) contradict existing experimental data (19). Furthermore, particular care was taken to avoid overshooting during the final stages of the base addition; none of the samples was ever at a pH higher than 8.25.

(3) The precipitates may form during the TEM sample preparation. This explanation seems unlikely because for the $\Gamma = 1.59$ sample, the most undersaturated sample in which precipitates were observed, the XAFS were collected both wet and dry with exactly the same results. The drying procedures for the TEM and XAFS sample preparation were similar, since both involved rapid drying at room temperature in an inert atmosphere. Also, since for this sample 99% of the Co in solution was taken up by the solid in the titration, only a negligible amount of Co remained in solution to be available for precipitation.

(4) The surface may act as a site for nucleation. No doubt this does occur, but if the solution is undersaturated with respect to the precipitate phase, the nuclei which form will be unstable and will not grow, unless there is some other effect acting to reduce the activity of Co(II) in the solid phase.

In the background section, it was shown that changes in the properties of the aqueous solution and its constituent ions in the vicinity of the interface cannot induce precipitation. In contrast, the other models discussed, including the surface energy model, the dropwise base addition model, and the solid solution model of Farley *et al.* (4), can provide valid bases for surface precipitation. The surface energy model, however, cannot explain the morphology of the precipitate particles in relation to the Al_2O_3 grains. If minimization of total surface energy were the driving force, we would expect the precipitate to form in one of two morphologies, depending on the relative magnitude of the various surface energy terms (see Eq. [2]): as a coating, or filling in cracks and pores with high radius of curvature. In the first case, the coating would be expected to cover the maximum possible amount of surface and therefore be as thin as possible, to the point where it would be less than a monolayer thick—the exact situation which would properly be called ''adsorption.'' In fact, no evidence has been found for coatings on Al_2O_3 grains, either of $Co(OH)_2(s)$ or anything else. The TEM does not provide evidence for the precipitates filling in zones of high surface curvature, either; instead, the precipitates seem to form as discrete particles within the pores of the Al_2O_3 matrix. We thus reject the possibility that reduction of surface energy could be inducing precipitation.

Note also that effects of a nearby Al_2O_3 interface on the properties of a solid precipitate, such as an electric field effect on a polarizable solid, will in general be confined within some finite distance of the interface (in most cases this distance should be small, i.e., no more than a few nanometers). Thus, from a thermodynamic viewpoint, these effects may also be described in terms of surface energies.

Effects of this type will result from the relaxation of the assumption that there is no net change in free energy on transport of the solid from the bulk solution region to the interface region (ΔG_3, in Fig. 2). The effects the presence of the interface has on the properties of the solid should have the same morphological consequences as any other factors contributing to the surface energy. Consequently, the lack of TEM evidence for precipitates coating Al_2O_3 particles or filling cracks and pores also lends support to the assumption that there is no free energy change on moving the solid precipitate into the interface region.

The kinetic effect of dropwise base addition is another possible explanation for the precipitates seen in this study. If this effect were causing precipitation, however, some other kinetic effect would be preventing dissolution of the precipitates during the 5 days of equilibration, the minimum titration time for samples in this study. In blank solutions (i.e., with no powder), any precipitates that form were observed to dissolve immediately. One other point worth noting is that the downward pH drift that was observed in the sorption sample titrations is exactly the opposite from the trend that would be expected if the drift were caused by gradual dissolution of $Co(OH)_2$. Given these facts, it seems unlikely that dropwise addition of base is the root cause of precipitation in our samples. It may be, however, that the localized pH shock that occurs at the drop interface allows the formation of a stable precipitate phase that might otherwise be kinetically prevented from occurring during the time scale of the experiment.

A more complex analysis is required to determine whether the formation of a solid solution could be causing surface precipitation in this system. In the solid solution model of Farley *et al.* (4) an ideal solid solution is assumed, so the activity of the sorbing component in the precipitate phase is equal to its mole fraction; that is,

$$a_i = X_i. \qquad [14]$$

For the $\Gamma = 1.59$ sample, the ion activity product of Co^{2+} and OH^- ions is only 2% of the value required to precipitate the most stable form of $Co(OH)_2(s)$. Thus, the mole fraction of $Co(OH)_2$ in the solid solution can be at most 0.02. This is a possibility that may be clearly rejected on the basis of the XAFS data; if it were true, the second-neighbor backscattering would be dominated by Al rather than Co.

Another possibility is that the two components (i.e., $Co(OH)_2$ and $Al(OH)_3$) form a solid solution that is not ideal. In fact, this is much more likely than an ideal solid solution, given that close approaches to ideality are extremely rare, and in any case would be unlikely over the complete range of concentrations for two end members with different structures. Farley *et al.* point out that an ideal solution is not the only possibility, merely a simple and systematic way of implementing the idea that a solid solution forms.

In nonideal solid solutions, the activity coefficient for a given component can be less than or greater than 1 instead of being equal to 1; i.e., the deviation from ideality can be either negative or positive. If the two components bind more strongly to each other than to themselves, the deviation from ideality is positive. As the positive deviation increases, at some point a compound of the two will be more stable than the solid solution. Therefore, if ternary compounds form along the $Co(OH)_2$–$Al(OH)_3$ pseudobinary, it would indicate the there is a positive deviation from ideality; i.e., a precipitate would form more easily than in the ideal case at any particular mole fraction of Co. While the CoO–Al_2O_3–H_2O phase system has not received much study, more information is available on the analogous system MgO–Al_2O_3–H_2O. Mg^{2+} has an ionic radius similar to Co^{2+} (0.72 Å vs 0.745 Å (54)) and both $Mg(OH)_2$ and $Co(OH)_2$ crystallize in the brucite structure. The results of a study of phase stability in the $Mg(OH)_2$–$Al(OH)_3$ system (Fig. 13a) (55) show that a double-hydroxide phase does form and also that there is a limited solubility of Al^{3+} in $Mg(OH)_2$. At room temperature, the proposed double-hydroxide phase has the stoichiometry $AlMg_2(OH)_7$. Extrapolating to the $Co(OH)_2$–$Al(OH)_3$ system, these results imply that the deviation from ideality is positive.

Based on the work on the $Mg(OH)_2$–$Al(OH)_3$ system, it seems that any phase containing both $Co(OH)_2$ and $Al(OH)_3$ is unlikely to be an ideal solid solution. If the solubility of Al^{3+} in $Co(OH)_2$ is limited to a few percent, as in $Mg(OH)_2$, in order for precipitation of a solid solution to have occurred in the $\Gamma = 1.59$ sample, the activity coefficient of Co in the solid phase would have to be approximately 0.02. In the case of the brucite-structure phase (i.e., $Co(OH)_2(s)$), however, this activity coefficient would violate the thermodynamic principle that Raoult's law must be obeyed by a component of a solution as its mole fraction approaches 1; i.e.,

$$\lim_{X_i \to 1} \gamma_i = 1. \qquad [15]$$

A schematic illustration of how the activity of $Co(OH)_2$ is likely to vary with concentration is shown in Fig. 13b. The activity would be expected to be approximately equal to the concentration in the $Co(OH)_2(s)$ end member phase, but would be much lower in the double-hydroxide phase.

The remaining possibility is that the precipitate is a double-hydroxide phase, analogous to the double hydroxide proposed by Mascolo *et al.* (55) for the $Mg(OH)_2$–$Al(OH)_3$ system, and, perhaps, to the clay-like structures proposed by Charlet and Manceau (28) for sorption on silicates. Recent work has shown that at high concentra-

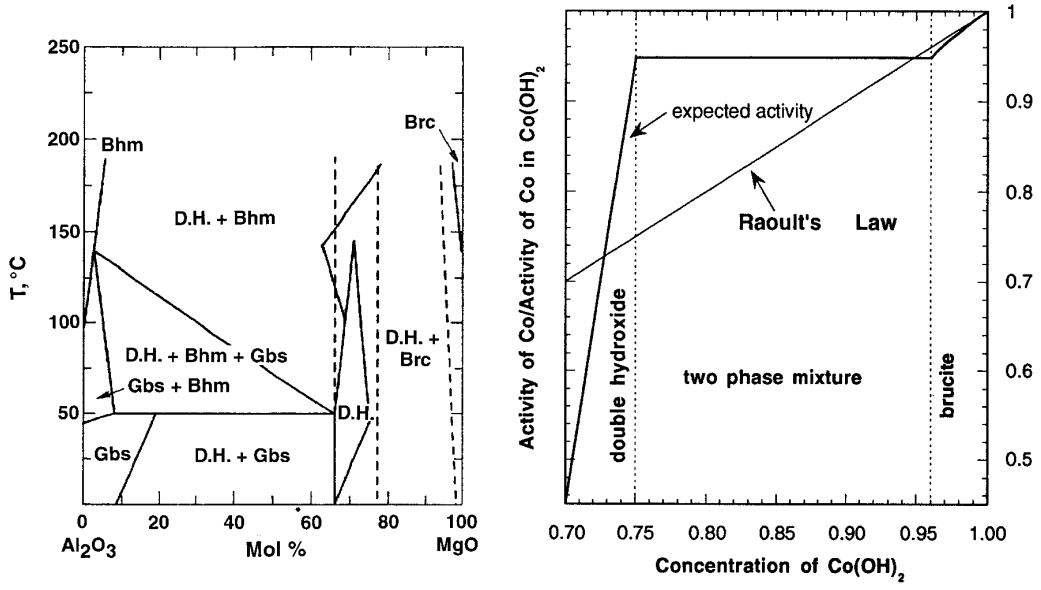

FIG. 13. (a) Phase diagram of $Mg(OH)_2$–$Al(OH)_3$ system, whose phase behavior should be similar to that of the $Co(OH)_2$–$Al(OH)_3$ system. Bhm stands for boehmite, Gbs for gibbsite (different polymorphs of $Al(OH)_3$), Brc for brucite ($Mg(OH)_2$), and D.H. for double hydroxide (from Mascolo *et al.* (55)). (b) Schematic illustration of the Co activity variation with molar concentration of $Co(OH)_2$, assuming phase behavior is similar to that illustrated for $Mg(OH)_2$–$Al(OH)_3$ in (a).

tions and in the presence of ammine, impregnation of γ-Al_2O_3 catalyst supports with Co(II) results in the formation of a hydrotalcite structure (56) of stoichiometry $[Co_{0.66}Al_{0.34}(OH)_2](CO_3)_{0.17}\cdot 0.61H_2O$. The hydrotalcite structure has metal hydroxide layers which are identical to the brucite structure but with a third or more of the Mg(II) replaced by Al; anions such as carbonate, nitrate, and chloride (as well as water molecules) in the interlayer space compensate the excess charge.

The coprecipitation experiment was designed to test whether the precipitation seen in the sorption samples might be caused by the formation of a double-hydroxide phase. Since the two separate Co(II) and Al(III) solutions were undersaturated before mixing and were diluted by another factor of 2 when they were mixed, the fact that a precipitate formed and persisted is definitive evidence for the existence of a stable ternary-hydroxide phase. The similarity of the Co EXAFS and XANES of the coprecipitate and the sorption samples (Fig. 6) strongly suggests that it is in fact the double hydroxide which is responsible for precipitation in the sorption samples. We conjecture that the double-hydroxide coprecipitate forms as Al(III)(aq) is gradually produced by dissolution of alumina. In addition to accounting for the XAFS, this process would account for the slow downward drift in pH seen in the sorption titration, as Co(II) is removed from solution to form a hydroxide precipitate.

Quantitative fitting of the EXAFS shows that the Co in the coprecipitate has more Al second-neighbors than in the sorption samples. This suggests that the double-hydroxide phase can have a range of possible stoichiometries, as was also found in the $Mg(OH)_2$–$Al(OH)_3$ system (55). The fit of the EXAFS for the coprecipitate indicates that there is amplitude cancellation between the Al and Co contributions to the second-shell scattering. One consequence of this cancellation is that small numbers of Al second-neighbors cannot be distinguished in the EXAFS analysis. However, an increased proportion of the total second shell backscattering coming from Al in the lower surface concentration samples may cause the anomalously low Debye-Waller factors seen in the fits for these samples. It seems likely that the presence of Al in the coprecipitate and surface precipitates is responsible for their structures being different from that of β-$Co(OH)_2$(s).

Comparison of this result with the work by d'Espinose de la Caillerie *et al.* (56) would suggest that the phase we observe in both the coprecipitate sample and the higher coverage sorption samples has a hydrotalcite-like structure, with charge balance being accomplished by intercalation of nitrate ions (or possibly carbonate ions, which may be present at low levels even in the controlled atmosphere of the glove box) in the interlayer space. However, our XPS data rule out the presence of either nitrate or carbonate at the concentrations required to produce a hydrotalcite-type phase of the stoichiometry they describe. Work by Taylor confirms that Co(II) and Al(III) can form a double-hydroxide coprecipitate under conditions where CO_2 is excluded (57).

Further information about the mechanism of precipitation is provided by comparing the results of this work with our past

work on sorption of Co(II) on single crystal wafers of α-Al_2O_3 (58). In that study, we found that when Co adsorbed onto α-Al_2O_3 surfaces from cobalt nitrate solution at the same pH and Co concentration as in the present study, there was no significant clustering or formation of any local structure similar to $Co(OH)_2(s)$. In that study the solutions were preequilibrated before the insertion of the wafers, which could explain the dramatically different sorption behavior. Since the wafers were only equilibrated in the solutions for about an hour, there was no opportunity for Al_2O_3 to dissolve to form Al(III) in solution.

Certain other XAFS studies of Co(II) sorption, notably those that used TiO_2 as a substrate, have found little evidence of Co clustering (1, 30). It has been suggested that differences in the atomic structure and local bonding requirements between rutile and other sorbates could be responsible for the dramatic difference in the sorption behavior (30). Based on our results, it seems likely that one cause for the Co/TiO_2 result is that rutile is much less soluble in the pH range of the equilibration than are the Al_2O_3 (this study, 15, 17)), kaolinite (46), and SiO_2 (30) sorbents used in the present work and other studies.

Although formation of a coprecipitate may be the best explanation for surface precipitation in this work, it is not necessarily the cause of surface precipitation in all systems. In particular, the HFO material used in several studies is much less soluble than Al_2O_3, and hence may be less likely to act as a source of ions for the formation of a coprecipitate. There are, however, other differences between the HFO solid and the one used in this study. For example, it is so highly porous (surface area of 256 m^2/g) that essentially the entire solid is made up of surface, and, for the Charlet and Manceau study (21), the substrate and sorbate ions (Cr(III) and Fe(III)) have the same charge and ionic radius. As a result, it may not be surprising that the Farley *et al.* ideal solid solution model can explain the surface precipitation seen in that system, but not in the Co(II)/Al_2O_3 system.

CONCLUSIONS

It has been determined that Co(II) sorbs on Al_2O_3 in two modes: as a disordered, hydrous, surface-induced precipitate at the highest sorption densities, and as small complexes at lower sorption densities, confirming earlier suggestions that changes in sorption mode take place with changes in surface loading (1, 3). The complexes seen at the low sorption density include multinuclear complexes that may be analogous to those that have been postulated to exist in Co(II) solutions, though under the conditions of the experiment the solution phase is essentially free of multinuclear species.

The solutions from which the surface precipitates formed were in most cases not saturated with respect to $Co(OH)_2(s)$. Precipitation is shown to occur via the formation of a Co–Al double hydroxide, which is more insoluble than either $Al(OH)_3$ or $Co(OH)_2$. Evidence both from high-resolution TEM and from XAFS suggests that the precipitate phase has a structure which is similar to that of cobalt hydroxide solid, but is highly defected and contains a significant fraction of Co vacancies. The missing Co ions could be charge-balanced by substitution of Al^{3+} for Co^{2+}, as well as, perhaps, by H_2O molecules for OH^- ions. While the precipitate phase is associated with the Al_2O_3 substrate, it does not form a coating and there is no evidence for an epitaxial relationship between the precipitate and the substrate.

From a practical standpoint, these results have several implications. In the preparation of catalysts, the readiness with which precipitates form means that a uniform dispersion of metal ions across an oxide surface will be harder to obtain than previously thought, based on a more traditional view of sorption. Furthermore, on annealing, it is quite likely that a substantial fraction of the sorbed material will end up in forms other than the active phase. However, an understanding of the factors which cause surface precipitation should make it possible to design procedures that prevent the process from occurring.

For geochemical modelers or others who are interested in using laboratory data to predict uptake in less controlled environments, our findings indicate that coprecipitation of poorly characterized multicomponent phases may be a significant cause of sorption, particularly under conditions where the concentration of metal ions in the aqueous solution is fairly high. If this effect is recognized as being important, studies seeking to measure true adsorption processes should be able to prevent coprecipitation by making fairly simple changes in experimental design. Some possible measures would be to minimize the time in which the solid sorbent is in contact with the supernatant, to use the most insoluble sorbent possible, and to use the lowest possible concentration of metal ion.

The effects of coprecipitation, however, are not limited to laboratory systems—natural environments too will often have near-saturation concentrations of relatively insoluble ions such as Al(III). In areas near the source of a contaminant, where its concentration is high, coprecipitation of ternary (or higher order) phases may be the dominant mechanism acting to segregate aqueous contaminants to solid phases. To quantitatively model uptake under these conditions, it will be critical to find out which phases may be important in controlling the sorption of particular contaminants and to determine the solubility of these compounds as functions of pH and the concentration of the component species.

ACKNOWLEDGMENTS

We especially thank Dr. Per Persson for his aid in preparing samples and for his advice throughout this work. We also thank Dr. Ann Marshall for her help and expertise in the TEM work, Professors Mike Kelly and David Barnett for useful discussions about the XPS analyses, and the SSRL staff for their help at the synchrotron. We are grateful to current and past members of the Brown and Parks research group for their help in the XAFS data collection. This work was supported by the Department of Energy

through Grant DE-FG03-93ER14347. SSRL is supported by the Department of Energy (Chemical Sciences and Materials Science) and by the National Institutes of Health.

REFERENCES

1. Chisholm-Brause, C. J., O'Day, P. A., Brown, G. E., Jr., and Parks, G. A., *Nature* **348,** 528–530 (1990).
2. Katz, L. E., and Hayes, K. F., *J. Colloid Interface Sci.* **170,** 477–490 (1995).
3. Katz, L. E., and Hayes, K. F., *J. Colloid Interface Sci.* **170,** 491–501 (1995).
4. Farley, K. J., Dzombak, D. A., and Morel, F. M. M., *J. Colloid Interface Sci.* **106,** 226–242 (1985).
5. Sposito, G., ''The Surface Chemistry of Soils.'' Oxford University Press, New York, 1984.
6. Stumm, W., and Wieland, E., *in* ''Aquatic Chemical Kinetics'' (W. Stumm, Ed.), pp. 367–400. Wiley-Interscience, 1990.
7. Leckie, J. O., and Tripathi, V. S., ''Effect of geochemical parameters on the distribution coefficient, K_d.'' *in* 5th International Conference on Heavy Metals in the Environment, 1985.
8. Benjamin, M. M., *Environ. Sci. Tech.* **17,** 686–692 (1983).
9. Vordonis, L., Akratopulu, A., Koutsoukos, P. G., and Lycourghiotis, A. ''Developments of Methods for Regulating the Charged Surface Groups of γ-Al_2O_3 in Aqueous Solutions,'' *in* Preparation of Catalysts IV: Scientific Bases for the Preparation of Heterogeneous Catalysts. Louvain-La-Neuve, Elsevier Science Publishers, 1986.
10. Spanos, N., Kordulis, C. H., and Lycourghiotis, A., ''Development of a Methodology for Investigating the Adsorption of Species Containing Catalytically Active Ions on the Surfaces of Industrial Carriers,'' *in* Preparation of Catalysts V. Louvain-La-Neuve, Elsevier Science Publishers, 1990.
11. Brunelle, J. P., *Pure Appl. Chem.* **50,** 1211–1279 (1978).
12. Parfitt, G. D., *Croat. Chem. Act.* **45,** 189–194 (1973).
13. Fendorf, S. E., Sparks, D. L., Fendorf, M., and Gronsky, R., *J. Colloid Interface Sci.* **148,** 295–298 (1992).
14. Feitknecht, W., and Hartmann, L., *Chimia* **8,** 95 (1954).
15. Gayer, K. H., and Garrett, A. B., *J. Am. Chem. Soc.* **72,** 3921–3923 (1950).
16. Hayes, K. F., Katz, L. E., and Penner-Hahn, J. E., *in* ''SSRL Activity Report—1992,'' (A. Bienenstock, H. Winick, and K. Cantwell, Eds.), pp. 79–82. Stanford Synchrotron Radiation Laboratory, 1992.
17. Chisholm-Brause, C. J., Brown, G. E., Jr., and Parks, G. A., *in* ''XAFS VI'' (S. S. Hasnain, Ed.), pp. 263–265. Ellis Horwood Publishers, 1991.
18. Chisholm-Brause, C. J., Ph.D. thesis, Stanford University, 1991.
19. Sposito, G., *in* ''Geochemical Processes at Mineral Surfaces'' (J. A. Davis and K. F. Hayes, Eds.), pp. 217–228. ACS Symposium Series, American Chemical Society, 1986.
20. Baes, C. F., and Mesmer, R. E., ''The Hydrolysis of Cations.'' John Wiley & Sons, New York, 1976.
21. Charlet, L., and Manceau, A., *J. Colloid Interface Sci.* **148,** 443–458 (1992).
22. Bleam, W. F., and McBride, M. B., *J. Colloid Interface Sci.* **103,** 124–132 (1985).
23. James, R. O., and Healy, T. W., *J. Colloid Interface Sci.* **40,** 53–64 (1972).
24. Tewari, P. H., and Lee, W., *J. Colloid Interface Sci.* **52,** 77–88 (1975).
25. Scheidegger, A. M., Lamble, G. M., and Sparks, D. L., *Environ. Sci. Technol.* **30,** 548–554 (1996).
26. Dzombak, D. A., and Morel, F. M. M., *J. Colloid Interface Sci.* **112,** 588–598 (1986).
27. Kinniburgh, D. G., and Jackson, M. L., *in* ''Adsorption of Inorganics at Solid–Liquid Interfaces'' (M. A. Anderson and A. J. Rubin, Eds.), pp. 91–160. Ann Arbor Science, 1981.
28. Charlet, L., and Manceau, A., *Geochim. Cosmochim. Act.* **58,** 2577–2582 (1994).
29. O'Day, P. A., Brown, G. E., Jr., and Parks, G. A., *J. Colloid Interface Sci.* **165,** 269–289 (1994).
30. O'Day, P. A., Chisholm-Brause, C. J., Towle, S. N., Parks, G. A., and Brown, G. E., Jr., *Geochim. Cosmochim. Act.*, in press.
31. Ananthapadmanabhan, K. P., and Somasundaran, P., *Colloids Surfaces* **13,** 151–167 (1984).
32. Gaskell, D. R., ''Introduction to Metallurgical Thermodynamics,'' 2nd ed. McGraw-Hill, New York, 1981.
33. George, G. N., ''EXAFSPAK.'' Stanford Synchrotron Radiation Laboratory, 1993.
34. Rehr, J. J., and Albers, R. C., *Phys. Rev. B* **41,** 8139–8149 (1990).
35. Rehr, J. J., Mustre de Leon, J., Zabinsky, S. I., and Albers, R. C., *J. Am. Chem. Soc.* **113,** 5135–5140 (1991).
36. Rehr, J. J., Zabinsky, S. I., and Albers, R. C., *Phys. Rev. Lett.* **69,** 3397 (1992).
37. Zabinsky, S. I., Rehr, J. J., Ankudinov, A., Albers, R. C., and Eller, M. J., *Phys. Rev. B* **52,** 2995–3006 (1995).
38. Paces, T., M.S. thesis, Stanford University, 1968.
39. Yopps, J. A., and Fuerstenau, D. W., *J. Colloid Sci.* **19,** 61–71 (1964).
40. Hayes, K. F., Redden, G., Ela, W., and Leckie, J. O., *J. Colloid Interface Sci.* **142,** 448–469 (1991).
41. Papelis, C., Ph.D. thesis, Stanford University, 1992.
42. Furrer, G., and Stumm, W., *Geochim. Cosmochim. Acta* **50,** 1847–1860 (1986).
43. Battye, F. L., Jenkin, J. G., Liesegang, J., and Leckey, R. C. G., *Phys. Rev. B* **9,** 2887–2893 (1974).
44. Seah, M. P., and Dench, W. A., *Surface Interface Anal.* **1,** 2–11 (1979).
45. Tewari, P. H., and McIntyre, N. S. (Eds.), pp. 134–137. AIChE Symposium Series, 1975.
46. O'Day, P. A., Rehr, J. J., Zabinsky, S. I., and Brown, G. E., Jr., *J. Am. Chem. Soc.* **116,** 2938–2948 (1994).
47. Tröger, L., Arvanitis, D., Baberschke, K., Michaelis, H., Grimm, U., and Zschech, E., *Phys. Rev. B* **46,** 3283–3289 (1992).
48. O'Day, P. A., Brown, G. E., Jr., and Parks, G. A., *in* ''XAFS VI'' (S. S. Hasnain, Ed.), pp. 260–262. Ellis Horwood, 1991.
49. Greaves, C., and Thomas, M. A., *Acta Cryst.* **B42,** 51–55 (1986).
50. Bode, H., Dehemelt, K., and Witte, J., *Electrochem. Act.* **11,** 1079 (1966).
51. McEwen, R. S., *J. Phys. Chem.* **75,** 1782 (1971).
52. Matijevic, E., Mathai, K. G., Ottewill, R. H., and Kerker, M., *J. Phys. Chem.* **65,** 826–830 (1960).
53. Chisholm-Brause, C. J., Hayes, K. F., Roe, A. L., Brown, G. E., Jr., Parks, G. A., and Leckie, J. O., *Geochim. Cosmochim. Acta* **54,** 1897–1909 (1990).
54. Shannon, R. D., *Acta Cryst.* **A32,** 751–767 (1976).
55. Mascolo, G., Marino, O., and Cantarelli, A., *Trans. J. Br. Ceram. Soc.* **79,** 6–10 (1980).
56. d'Espinose de la Caillerie, J.-B., Kermarec, M., and Clause, O., *J. Am. Chem. Soc.* **117,** 11471–11481 (1995).
57. Taylor, R. M., *Clay Min.* **19,** 591–603 (1984).
58. Towle, S. N., Bargar, J. R., Brown, G. E., Jr., Parks, G. A., and Barbee, T. W., Jr., *in* ''Structure and Properties of Interfaces in Ceramics'' (D. A. Bonnell, U. Chowdhry, and M. Rühle, Eds.), pp. 23–28. Materials Research Society Symposium Proceedings, Materials Research Society, 1995.